Experimental and Theoretical Analysis of Fast Neutron Spectra

H. van Dam

EXPERIMENTAL AND THEORETICAL

ANALYSIS OF FAST NEUTRON SPECTRA

EXPERIMENTAL AND THEORETICAL

ANALYSIS OF FAST NEUTRON SPECTRA

PROEFSCHRIFT

ter verkrijging van de graad van
doctor in de technische wetenschappen
aan de Technische Hogeschool Delft,
op gezag van de Rector Magnificus
ir. H.R. van Nauta Lemke, hoogleraar in
de Afdeling der Elektrotechniek, voor een
Commissie uit de Senaat te verdedigen op
woensdag 23 juni 1971 te 1400 uur

door

Hugo van Dam
natuurkundig ingenieur
geboren te Surabaia

1971
Afdeling der Technische Natuurkunde
van de Technische Hogeschool te Delft

Dit proefschrift is goedgekeurd door de

promotor prof. dr. J.J. Went.

Aan mijn Ouders

Aan Elly, Marion en Petra

CONTENTS

I INTRODUCTION

During the first decade of the nuclear energy era almost all research effort was concentrated on the development of nuclear reactors with a neutron cycle based on thermalization of fast neutrons liberated by fission of ^{235}U. This is due to the fact that, as a consequence of the nuclear properties of the uranium isotopes, a self-sustaining chain reaction in a system fuelled with natural or slightly enriched uranium can be achieved only if moderating material is added.

As soon as enriched uranium and plutonium became available it was possible to develop reactor cores with a high concentration of fissile material and a low concentration of moderating material. This can be profitable from the point of view of fuel economics because, due to an appreciable hardening of the neutron spectrum, the average number of neutrons emitted per neutron absorbed in fissile material increases thereby enhancing the number of neutrons available for conversion of fertile material (Th^{232} or U^{238}) into fissile material (U^{233} or Pu^{239}).

With a sufficiently hard neutron spectrum in the core the number of excess neutrons available for conversion of non-fissile isotopes is such that a net increase of fissile material in the system can be achieved (breeder reactor), thereby providing the nuclear fuel required to meet a growing demand for energy and to guarantee the future energy demand of mankind. The fuel inventory in a fast reactor, however, considerably exceeds the amount of fuel in a thermal system due to the decreasing absorption probability for neutrons with increasing energy.

This means that for economical reasons a high core power density is required giving rise to technological problems, e.g. concerning thermo-hydraulics and material behaviour at high fast neutron fluences. Another important aspect concerns the safety problems of a fast reactor, which are partly related to the neutronic behaviour. Due to the very short mean generation time of neutrons in a fast core in comparison to thermal systems there is a strong need both for very fast safety mechanisms based on the neutronic behaviour of the system and the avoidance of positive reactivity in case of failure of components.

Because gradually a sufficient amount of plutonium bred in thermal systems becomes available for the start-up of a generation of fast reactors there is a strong incentive for basic research on the neutronic behaviour of fast reactors and in fact an important part of the experimental and theoretical work in reactor physics nowadays is concentrated on this field.

As already indicated the important characteristics of a fast reactor are related to the energy distribution of the neutrons; this distribution is governed by the different incore neutron processes and depends on the material and geometrical composition of the system. In fact all fundamental reactor physics studies are directed towards an accurate prediction of energy and spatially dependent neutron reaction rates in relation to a number of parameters such as system lay-out and dimensions, fuel distribution, control-rod positions, temperature, coolant density and burn-up.

Both experimental and theoretical studies of fast neutron spectra are required for gaining an insight into this rather complex problem. In this thesis a report is given of the research in this field as started a few years ago at the Interuniversity Reactor Institute at Delft.

In the second Chapter a survey is given of the experimental aspects, starting with a description of FANCY, an assembly designed for fast spectrum studies with a modest amount of fissile material. In the next paragraphs some methods used for the incore measurement of spectra are outlined together with the data handling by means of a computer and some important electronical aspects of the detection system.

The third Chapter comprises the numerical aspects of the transport equation and the principles of some computer codes developed for calculation of space-dependent neutron spectra; special attention is paid to the treatment of anisotropic scattering.

The next chapter deals with the evaluation of group cross sections for fast reactors in connection with the discretization of the energy variable in numerical transport calculations.

Because generally this forms an important aspect of the calculation of spectra the composition of the FANCY-assembly has been selected in such a way as to introduce large discrepancies between calculated and measured spectra in case of incorrectly evaluated group cross sections.

Chapter IV is concluded with a consideration of the possibility of deducing data pertinent to group parameters from measured neutron spectra.

In the last chapter results are presented of the experimental work together with an analysis of information inferred from the experiments in correlation with theory.

II EXPERIMENTAL ASPECTS

II.1 Fast neutron spectrum assembly

For experimental studies of fast neutron transport in matter it is often not necessary to use a fast critical system. In many cases even, it must be preferred to focus the attention on "clean" experiments, i.e. measurements in assemblies with simple geometry and material composition as well as a well-defined fast neutron source which can be obtained by using radioactive neutron sources or a very small amount (compared to the fuel investment in a critical system) of fissile material. This approach offers the flexibility to select the system parameters such that the influence of interfering effects on the particular phenomenon to be studied is either well-known or negligible. These considerations served for guidance when it was decided to study the influence of scattering cross section resonances on neutron energy distributions.

The assembly for fast neutron spectrum measurements FANCY (Fast Neutron Counting Assembly) is positioned on top of the thermal column of the 2 MW HOR pool reactor (see Fig. 1). FANCY consists of a core embedded in a graphite reflector with outside dimensions of 130x130x130 cm^3. The system is fed by the neutron current from the thermal column; the flux level of this neutron field can be varied by controlling the water level in a tank positoned underneath the assembly and is monitored by a neutron counter. The monitor counter is inserted in the reflector part of FANCY, in order to account for flux shifts caused by movement of the reactor shim rods.

An isomeric view of the FANCY-core is shown in Fig. 2. The core is formed by a square array of 100 vertical aluminium matrix tubes which are fixed to a bottom support; the lattice pitch is 54 mm. Different core compositions can be created by stacking 50.8x50.8 mm^2 (2x2 sq.in.) platelets of appropriate materials into the elements which have a wall thickness of 1 mm. For the experiments reported in this thesis use has been made made of aluminium platelets of 1/8 in. thickness; a total number of 17000 platelets was required to form a cuboidal core with 54 cm edges. In the upper section of the elements graphite

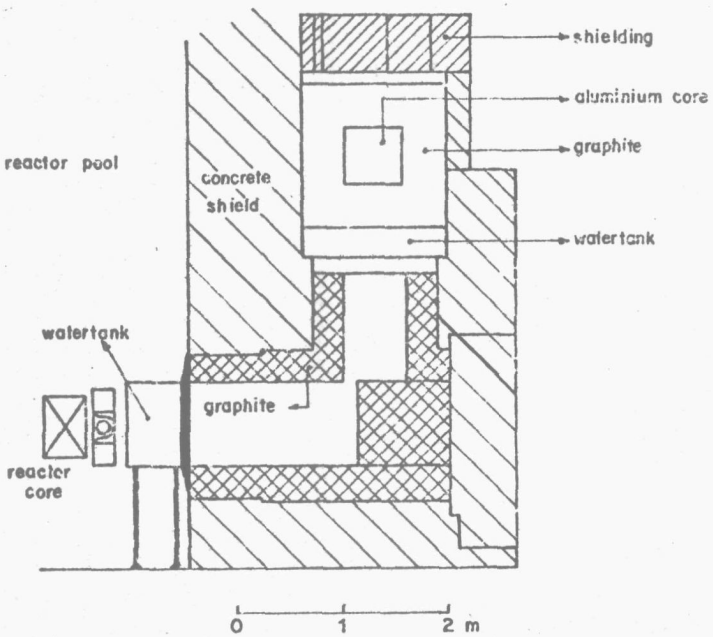

Fig. 1. Vertical cross sections along the axis of the thermal column of the HOR.

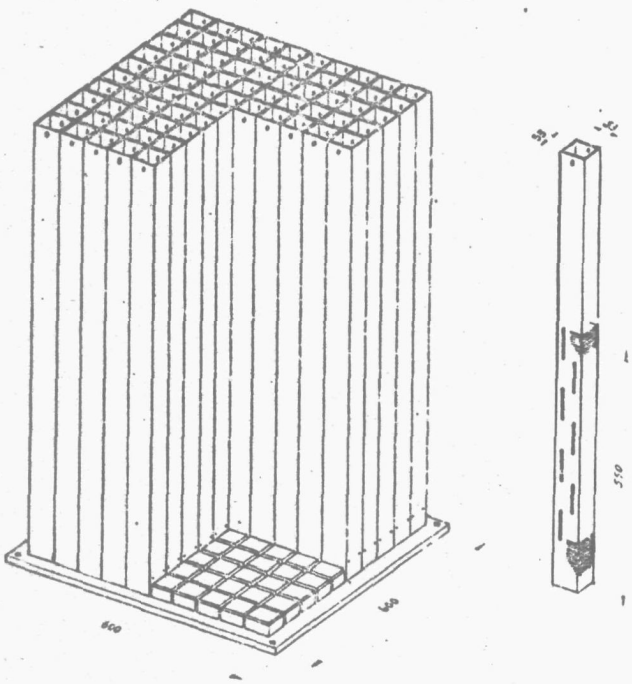

Fig. 2. Isomeric view of the FANCY-core.

blocks are inserted, forming a part of the reflector. Pseudo-cylindrical and spherical cores can be created by appropriate loading patterns.

Channels for insertion of counter tubes can be formed by using platelets and graphite blocks with a central hole, whereas in some platelets recesses have been machined for placing activation foils.

The top shielding of FANCY consists of a double rotating plug arrangement contained in a concrete block of 50 cm thickness. By means of this construction all necessary operations (core modifications or insertion of detectors) can be performed at maximum power level of the reactor, all lattice positions being accessible by means of combined rotations of the shielding plugs.

Because the object of the study was the comparison of theoretical predictions and experimental results, the experimentel conditions had to be chosen carefully. The most important restriction from theoretical point of view is imposed by the number of space variables that can be handled by the computer codes. In a strict sense every geometry that can be realized with the available means (fuel plates, amount of material) is three-dimensional; a geometrically exact calculation of spectra with a sufficient number of other variables (energy groups and, in the case of transport calculations, angular orientation of the neutron flight direction) is then possible only by using a computer with very large memory capacity and is rather time consuming. A system that can be treated by two-dimensional calculations with sufficient accuracy is obtained provided the dimension of the system in one of the coordinate directions is large when compared to the mean free path of neutrons. For thermal systems this can be realized in a simple way because of the small mean free path of thermal neutrons (on the order of 1 cm) and the possibility of introducing materials that absorb all thermal neutrons so as to obtain simple boundary consitions for the mathematical problem [Ca68]. For fast neutrons the amount of material needed for this approach is rather large whereas a spatial limitation is hindered by back-scattering of neutrons by the environment of the experimental assembly. Therefore a "one-dimensional approach",

based on an approximation of *spherical* symmetry, has been adopted for the work reported here.

A centrally located fission source is obtained by inserting uranium fuel plates, enriched to 90% in ^{235}U, symmetrically around the centre of the assembly. These fuel plates each contain 37.5±1.5 g of ^{235}U in the form of a 125x50x5 mm^3 platelet of a uranium-aluminium alloy encapsulated in aluminium. More than 99% of the reactor neutrons feeding the assembly have been completely thermalized before streaming into the core; as a consequence the ratio of fast neutron flux originating from the fission plates to the fast background flux originating from the reactor core is high enough to measure the first component with sufficient accuracy.

In some of the computer calculations the actual source geometry is approximated by an equivalent spherical shell source. This approximation is adequate for two reasons:

1. The arrangement of fuel plates can be chosen such as to make the difference between the mean distance from an arbitrary point inside the core to the actual source-surface and the same distance to the equivalent spherical source-surface small compared to the mean free path of fission neutrons in the core (4-10 cm).
2. In the energy range under about 0.5 MeV, where the mean free path of the neutrons at some energies is smaller the contribution of first-flight source neutrons to the total flux is small; because the collision processes result in a spatial smearing-out, the actual source geometry will have an even smaller influence on the space-energy distribution of neutrons.

The perturbation caused by back-scattering of neutrons from the concrete shielding has been avoided by selecting a reflector thickness consistent with a negligible contribution to the core flux of neutrons scattered back from outside the reflector. This has been checked by calculations of core neutron spectra for cases with varying reflector thicknesses; in this way it was ascertained that an increase of graphite reflector thickness does not influence the differential neutron flux at any energy or position inside the core by more than $1^{o}/oo$.

II.2 Methods used for incore spectrum measurements

II.2.1 Introduction

Fast neutron spectra were measured in the FANCY-core with the proton recoil technique using hydrogen and methane-filled spherical and cylindrical counter tubes. A short survey of the fundamental aspects of this technique will be presented here together with some special features of the approach for this project; for a detailed analysis of the operation characteristics of proportional counter tubes the reader is referred to literature [Pr64, Ki60].

II.2.2 Fundamental aspects

As a consequence of the kinematics of neutron-proton collisions, the energy distribution P(E) of recoil protons in a counter tube exposed to a mono-energetic neutron flux $\phi(E_o)$ is given by:

$$P(E) = N \cdot \sigma(E_o) \cdot \frac{\phi(E_o)}{E_o}, \quad \text{for } o \leq E \leq E_o,$$
$$= o \quad , \quad \text{for } E_o < E \quad , \qquad (2.1)$$

where

E_o = energy of the incident neutrons,
ϕ = flux in $n.cm^{-2}.s^{-1}$,
P(E) = number of recoil protons per unit energy per s,
N = number of protons in the sensitive volume of the counter tube,
$\sigma(E_o)$ = scattering cross section of protons in cm^2.

This response function is shown in Fig. 3 by the dotted line ("ideal response"). The response as measured with a complete detecting system, consisting of counter tube and pulse-amplifying electronics is given by the solid line (actual response"). The difference between actual and ideal response function is caused by four phenomena:

1. Statistics in the primary ionization created by protons together with fluctuations in the subsequent gas multiplication process in the counter tube;

these effects give a rounding-off at the right side of the response function which limits the energy resolution of the system.

2. Imperfections in counter design, e.g. variations of anode wire diameter and the limited compensation of electric field perturbations at both ends of the anode wire by means of field tubes [Ro49,Be70], giving rise to local variations in gas multiplication, and the presence of electropositive impurities in the filling gas. These phenomena give an additional broadening of the response function.
3. Electronic noise in the amplifying system, giving rise to the strong increase of the response curve at the left side, which imposes a lower limit to the useful energy range of the counter tube; the electronic noise also gives an additional rounding-off of the step curve at the right side.
4. Wall and end effects caused by the fact that recoil protons, as a consequence of their finite range in the gas filling, may leave the sensitive volume of the counter tube before loosing all their energy by means of ionization processes. This causes the slope of the response function in the intermediate part and limits the useful energy range of the counter tube at the high energy side.

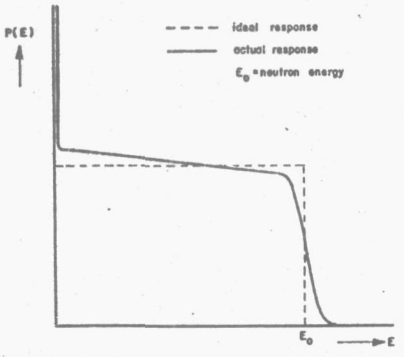

Fig. 3. Ideal and actual response of a proton recoil detector to monoenergetic neutrons.

The stochastic effects, mentioned under point 1 and 3 show a distribution which is approximately gaussian [Fa47,Fa66,Gi53] and therefore the response function at the right side has the shape of an error function. Although the phenomena mentioned under point 2 do not have a gaussian nature, their effect can be treated as an additional gaussian broadening.

The resolution that results from the combined effects is called the intrinsic width of the detection system and is defined as the full width at half peak maximum (FWHM) of the response function for monoenergetic protons; for a gaussian distribution this is equal to 2.36 times the standard deviation.
For the relative intrinsic width $\Delta E/E$ in percent the next formula may be derived [Be67]:

$$w_i^2 = A + \frac{B}{E^2} + \frac{4000}{E(keV)} \% \quad , \tag{2.2}$$

where

w_i = relative intrinsic width,
A = energy-independent term, due to mechanical imperfections,
$\frac{B}{E^2}$ = term for electronic noise.(neglected in Ref.Be67).

The last term refers to the statistics in the primary ionization and the gas multiplication process.
In practice w_i is on the order of 10%.

From Eq. (1) the following relations between neutron and proton spectrum are obtained:

$$P(E) = N \int_E^\infty \sigma(E') \, \phi(E') \, \frac{dE'}{E'} \tag{2.3}$$

or

$$\phi(E) = - \frac{E}{N\sigma(E)} \cdot \frac{dP(E)}{dE} \quad . \tag{2.4}$$

It must be emphasized that in Eq. (4) the proton spectrum, corrected for wall and end effects, must be substituted; this correction procedure is an important aspect of the data handling and will be analysed in more detail in paragraph II.3.

As can be seen from Eq. (4) the neutron spectrum is obtained by means of differentiation of the proton spectrum which implies an enhancement of relative statistical errors.

The continuous function P(E) is measured in discretized form as a number of counting results in energy channels, covering the energy interval of interest. The counting rate in each channel is governed by a Poisson distribution [Pr64], which means that the relative standard deviation of a number of counts n is given by $1/\sqrt{n}$. Numerical differentiation is based on subtraction of counting data in neighbouring channels, say n_1 and n_2 (numbered with increasing energy), giving a relative statistical standard deviation:

$$\sigma_{rel} = \frac{\sqrt{n_1+n_2}}{n_1-n_2} \quad , \tag{2.5}$$

which is in all practical cases larger than the relative statistical variances in n_1 and n_2.

In the previous analysis a slope-taking interval of one channel width only has been assumed. The statistical accuracy of the neutron spectrum may be increased either by measuring in channels with a greater energy width or by using a differentiation scheme based on a least-squares fit of the counting results in a greater number of neighbouring channels. In both cases the effective slope-taking interval is increased thereby deteriorating the energy resolution of the neutron spectrum obtained. This leads to an optimization problem which is illustrated in Figs. 4. and 5.

Around each measuring point in the neutron spectrum an error ellipse can be drawn with axes defined by the statistical variances in respectively energy and flux. The energy resolution as a function of slope-taking interval is given in Fig. 5; this part of the graph is taken from [Be67] and applies to the case where a straight-line least-squares fit is made to the measuring data in the slope-taking interval. The standard deviation σ_ϕ in Fig. 4. is determined by the number of counts in the slope-taking interval and is about inversely propertional to the square root of the interval width. From this relation it can be concluded that optimum conditions (i.e. minimum ellipse area in

Fig. 4.) are obtained with a slope-taking interval about equal to the intrinsic width (see Fig. 5.). For this slope-taking interval the energy-resolution obtained is only slightly worse than the intrinsic resolution.

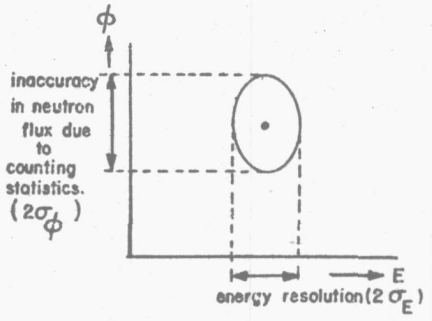

Fig. 4. Measuring point with error ellipse.

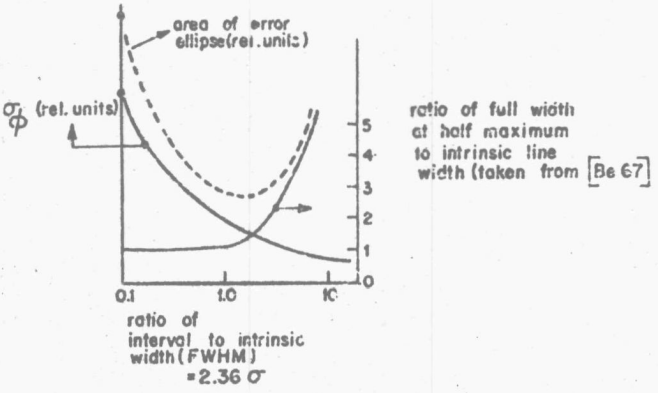

Fig. 5. Optimization of slope-taking interval (partially taken from [Be67]).

In practice the relative statistical inaccuracy σ_ϕ/ϕ is of the order of a few percents. In case the measured spectra are to be compared to calculated spectra, the accuracy is generally better. This is due to the fact that for the numerical calculation of spectra the energy variable is discretized in a number of energy groups (see Chapter III) which results in a number of group fluxes. Experimental group fluxes are obtained by integration of the measured spectrum over the energy intervals which reduces the inaccuracy introduced by the differentiation procedure outlined above. Therefore a statistical accuracy better than 1% in the measured group fluxes can be obtained.

II.2.3 Detector design and calibration

Both spherical and cylindrical counter tubes has been used for neutron spectrometry in FANCY. A cross-sectional view of these counter types is shown in Fig.6.

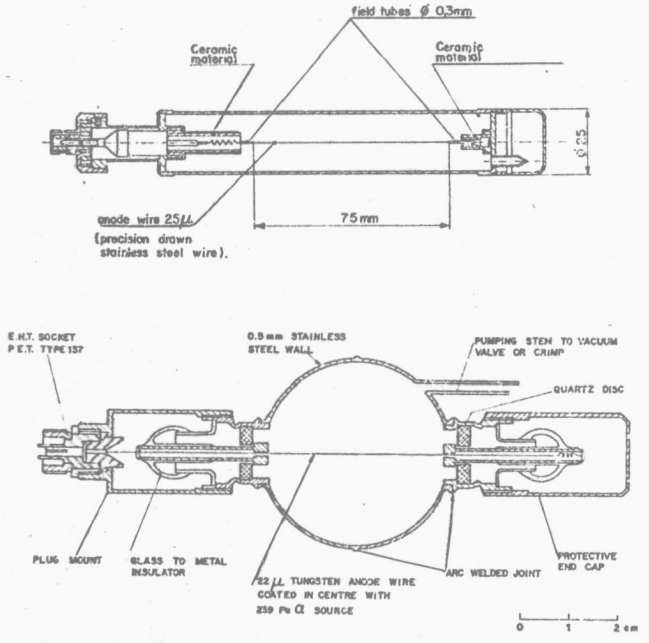

Fig. 6. Spherical and cylindrical proton recoil proportional counter.

The spherical detectors have been purchased from Centronix Works, England; the cylindrical ones were either home-made or purchased from Laboratorium Prof. Dr. Berthold, Wildbach, Germany. In all counter types the anode is 25 microns in diameter and made from precision-drawn stainless steel wire; the wire supports at both ends have been carefully dimensioned in order to obtain a well-defined sensitive counter volume with uniform gas multiplication. Compared to cylindrical detectors, which are easier to construct, spherical counters have the following advantages:

1. In anisotropic neutron fields the proton spectra are independent of the detector orientation.
2. There are no dead volumes at both ends of the anode wire; in cylindrical detectors recoil protons originating from the dead volume and entering the sensitive volume cause a spectral perturbation, which cannot be easily accounted for.

The energy resolution of cylindrical detectors is generally better because of the simpler dimensioning for uniform gas multiplication.

The gas filling of the detectors consists of either hydrogen or methane. The latter is used for measurements above 800 keV, where high stopping power for recoil protons is needed to avoid excessive wall effects (see II.3).

Energy calibration of the detectors was performed in different ways:

1. In the spherical detectors a trace of ^{239}Pu coating on the centre of the anode wire emits 5.15 MeV alpha particles; only a portion of the alpha particle energy is absorbed by the filling gas, depending on the gas pressure, and can be detected as a calibration peak in the energy spectrum. The calibration energies can be obtained from alpha range tables [An63].
2. In the cylindrical detectors a small amount of ^{3}He or nitrogen is added. This yields either 764 keV or 615 keV pulses when the counter is irradiated with thermal neutrons as a result of (n,p) reactions:

$$^{3}_{2}\mathrm{He} + ^{1}_{0}\mathrm{n} \longrightarrow {}^{1}_{1}\mathrm{p} + {}^{3}_{1}\mathrm{T} + 764\ \mathrm{keV}$$

$$^{14}_{7}\mathrm{N} + ^{1}_{0}\mathrm{n} \longrightarrow {}^{14}_{6}\mathrm{C} + {}^{1}_{1}\mathrm{p} + 615\ \mathrm{keV}\ .$$

By measuring the gas multiplication as a function of high voltage applied to the counter (see Fig. 7.) a proper setting of counter voltage for operation in the proportional region is obtained; a high gas multiplication is desirable to obtain high signal-to-noise ratios.

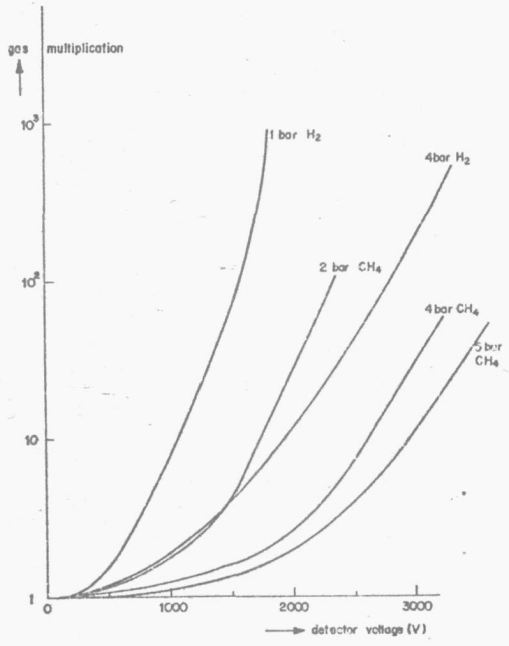

Fig. 7. Measured gas multiplication as a function of high voltage for different gas fillings (spherical detector).

For measurements in spectra with a thermal neutron component it can be disadvantageous to use ^{3}He or N as calibration gas in proton recoil detectors; in this case the detectors must be surrounded with cadmium during the actual measurements, which causes an increase of the gamma radiation level at the detector position due to thermal neutron capture. The use of ^{239}Pu has the advantages that calibration can be performed out-of-pile and can be verified during measurements without removing the detector from the assembly, because the calibration peak is well separated from the proton spectrum as a consequence of the high ionization density of the alpha particles.

In case methane is used as detector filling, the measured spectrum is a superposition of a proton-recoil and a carbon-recoil spectrum. For that case Eq. (2.4) must be modified [An67]:

$$\phi(E) = M(E) - \frac{5}{4} \cdot \frac{\sigma_c(5E)}{\sigma_H(E)} \cdot \phi(5E) \qquad (2.6)$$

where

$M(E)$ = flux spectrum calculated without accounting for carbon-recoils.
σ_c, σ_H = carbon resp. hydrogen scattering cross section.

This equation is based on the following assumptions:

1. Centre of mass system scattering is isotropic for carbon.
2. The relative (to protons) ionization created by a carbon fragment is about 0.75.

The correction term involves the value of the neutron flux at five times the energy at which the correction is made, which implies that the flux spectrum at energies above the useful energy range of the detector must be known. On the basis of the calculated spectra in FANCY the errors introduced if the carbon-recoil effect is being neglected, are found to amount to resp. 6%, 1.7% and 0.3% at neutron energies of 0.5 MeV, 1 MeV and 2 MeV.

II.3 Correction procedures for wall and end effects

Due to the finite dimensions of a counter tube, some of the recoil protons will leave the sensitive volume before having lost their total energy by means of ionizations inside this volume. Therefore not all amplitudes of the voltage pulses, detected as a consequence of the movement of electrons and ions in the electric field in the counter tube, are proportional to the initial energies of the recoil protons. The relation between the unperturbed and perturbed proton spectrum can be formulated as follows:

$$P(E) = \left\{P'(E) - \int_{E}^{\infty} P(E')K(E',E)dE'\right\} / \left\{1 - \int_{o}^{E} K(E,E')dE'\right\} \quad , \qquad (2.7)$$

where

$P'(E)$ = proton spectrum perturbed by wall and end effects,

$P(E)$ = unperturbed proton spectrum,

$K(E,E')dE'$ = probability that a recoil-proton with an initial energy E will be detected, as a consequence of wall or end effect, with an energy between E' and E'+dE'.

From Eq. (2.7) it follows that for the correction procedure both the correction function K(E,E') and the complete corrected proton spectrum above the energy E must be known. The second requirement cannot be fulfilled completely; two approximate methods can be applied:

1. Use can be made of the higher energy part of the spectrum, measured with detectors having a higher energy limit to the useful energy range, obtained for instance by increasing gas pressure or using methane instead of hydrogen, both giving a decrease in range of recoil protons, or by increasing counter-tube dimensions.
2. If only data from one measurement are to be used, the integral in the numerator of Eq. (2.7) can be replaced by

$$\int_{E}^{E_{max}} P(E')K(E',E)dE' \quad ,$$

where E_{max} is the upper limit of the measuring range. This gives an excess correction which increases with increasing E, i.e. P(E) is overestimated. The importance of the truncation error can be assessed however, by measuring P'(E) over a rather large energy

range in a great number of channels, say 200 or 400. The data in the upper part of the measuring interval are then used only to provide a better approximation for the integral in Eq. (2.7) for the lower part of the interval, whereas the truncation error can be assessed by varying E_{max}.

In the present work the last approach has been applied in order to avoid normalization problems and an extension of input data required for the numerical calculations associated with the first approach. For a particular case the errors caused by neglecting the influence of neutrons with an energy above E_{max} (the so-called "fast neutron effect") are shown in Fig. 8.

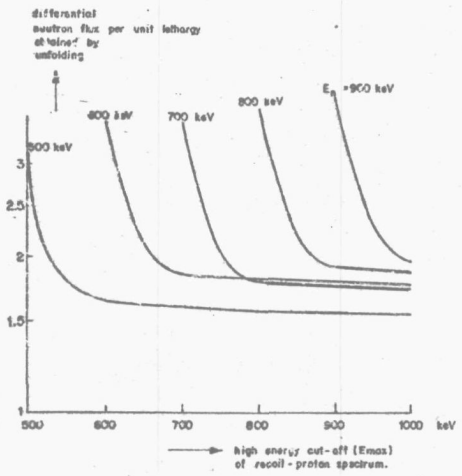

Fig. 8. Differential neutron flux as a function of the high energy cut-off of a measured recoil-proton spectrum.

The numerical calculation of the correction function K_i to be used in Eq. (2.7), is performed in two procedures. To develop these procedures three basic assumptions have been adopted:

1. The ionization tracks of protons in the gas filling are straight lines; this assumption is adequate because of the high ratio of proton-to-electron mass and the very small probability for high-angle "collisions" of protons with the coulomb field of the

nuclei in the counter gas [Pr64].

2. The counter tube is exposed to an isotropic neutron flux giving rise to an isotropic recoil-proton distribution. The influence of flux anisotropy is eliminated by using spherical counter tubes.
3. Only recoil protons born inside the sensitive volume are considered, i.e. the probability for protons, born inside the dead volumes at both ends, to enter the sensitive volume is taken to be zero. The influence of this effect decreases with increasing length-to-diameter ratio, which however, increases the influence of flux anisotropy on wall and end-effect corrections. The first procedure in the evaluation of $K(E,E')$ concerns the calculation of the track length distribution function $f(\ell)$, where $f(\ell)d\ell$ denotes the probability for recoil protons to have a distance between ℓ and $\ell+d\ell$ from the point of origin to the boundary of the sensitive volume. The distance is measured along the flight direction of the recoil protons which are assumed to be emitted homogeneously and isotropically inside the sensitive volume of the detector. The first assumption is always fulfilled as a consequence of the large mean free path of neutrons in the counter gas; the second assumption is relevant only for non-spherical counters and implies an isotropic neutron flux. As a consequence, the function $f(\ell)$ depends only on the geometry of the sensitive volume. From the definition of $K(E,E')$ the next relation holds:

$$K(E,E') = - \frac{df\ \{\ell(E) - \ell(E-E')\}}{dE'} \quad , \qquad (2.8)$$

where $\ell(E)$ = range of protons with energy E in the gas filling of the counter tube.

Obviously the function K depends on both geometry of the sensitive volume and gas filling parameters.

The distribution function $f(\ell)$ can be calculated either analytically [Sn67] or with a Monte-Carlo method. Computer codes based on both methods have been developed for the present work [Hu68]. Figure 9 shows some results for cylindrical counter tubes with length-to-diameter ratio equal to 1 respectively 2. In the Monte-Carlo

procedure the physical process is simulated by generating for each particle considered the cylindrical coordinates, determining point of origin and flight direction, by means of a stochastic procedure, and calculating the associated available path length ℓ; for the results shown in Fig. 9, 100.000 particles were considered for each Monte-Carlo calculation, in order to obtain a sufficient statistical accuracy, i.e. a mean standard deviation per track length interval of less than 2%; the calculation time for each case was 80 seconds.

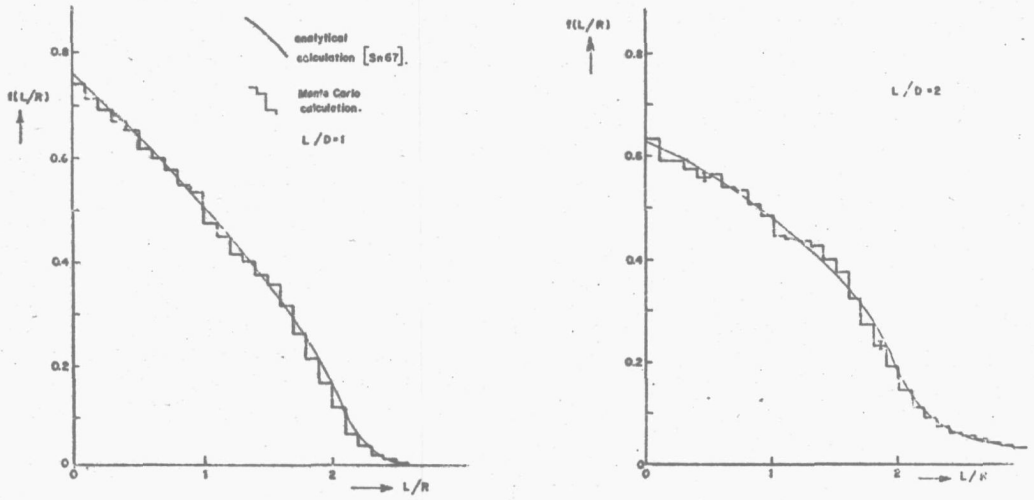

Fig. 9. Track length distributions for cylindrical detectors (length-to-diameter ratio = 1 resp. 2), calculated with analytical and Monte-Carlo methods.

For spherical detectors the track length distribution function has the form of a parabola:

$$f(\ell) = \frac{3}{4R} - \frac{3\ell^2}{16R^3} \qquad (2.9)$$

where

R = radius of the sensitive volume of the detector.

For the calculation of the neutron spectra according to Eq. (2.7) the values $\ell(E)$ have been obtained by

interpolation in the proton range-tables of Parker et al [Pa63].

All numerical procedures for the transformation of measured proton spectra into neutron spectra have been combined in an ALGOL-code PROSPER (proton spectrum reduction), designed for use on the Delft IBM 360/65 computer. In this code the slope-taking interval is taken about equal to the intrinsic resolution (FWHM) of the detector used, in accordance with the analysis presented in II.2.2.

II.4 Gamma discrimination and electronical aspects

In the preceding paragraphs it has been assumed that gas filled proton-recoil counters are sensitive to neutrons only. These detectors however, show gamma response due to ionization caused by electrons from gamma rays converted in the counter wall; gamma ray conversion in the counter gas contributes to a negligible extent because of the much lower density of the gas in comparison to the wall material. For a given counter size and gas pressure there exists an upper energy limit to the gamma response which is proportional to the maximum amount of ionization that can be deposited by conversion electrons in the counter gas. If the detector is used with conventional electronics, the useful energy range is rather limited due to gamma perturbation at low energies and wall-effect distorsion at high energies; some figures are given in Table I. These figures must be considered as indicative; in fact the lower energy limit is also dependent on the neutron-to-gamma ratio and the upper energy limit depends on the shape of the neutron spectrum and the method used for wall-effect corrections [Be68]. The data given in Table I refer to the VERA zero-energy assembly [Pa68]; the gamma-to-neutron ratio in this assembly is not indicated in literature. Benjamin states in [Be64] that a factor of 10 increase in gamma-to-neutron ratio increases by 30% the energy at which the gamma ray pulses are important. The energy of the *upper* energy limit in Table I is defined as the energy at which 40% of the recoil protons collide with the detector wall.

hydrogen filling pressure, bar	lower energy limit, keV	upper energy limit, keV
0.25	19	62
0.5	27	136
1.0	58	240
2.0	87	381
4.0	135	586
8.0	210	950

Table I. Useful energy range as a function of hydrogen filling pressure for a 3.94 cm diameter spherical proportional counter [Be64].

The useful energy range can be extended by applying pulse-shape discrimination in order to reject gamma pulses. This technique, introduced by Bennett [Be62], is based on the fact that the specific ionization (number of electron-ion pairs per unit track length) of conversion electrons is much lower than the density of ionization caused by recoil protons of the same energy. The rise time of the detector pulse depends on the length of the time interval during which the electrons arrive at the detector anode. This time interval is related to the length of the projection of the ionization track on a plane perpendicular to the anode wire.

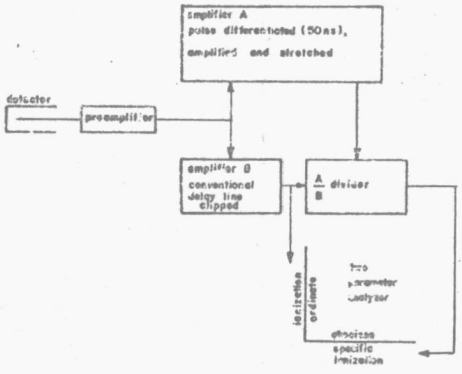

Fig. 10. Pulse shape discrimination circuitry used by Bennett [Be67].

As a consequence detector pulses originating from recoil protons will exhibit shorter rise times than those caused by conversion electrons. Figure 10 shows the elements of the pulse shape discrimination circuitry described by Bennett [Be67]. Each pulse from the counter is amplified and shaped by two amplifiers. The first produces a pulse with peak height proportional to the rate of rise of the incident pulse, by applying delay line differentiation with a time constant on the order of 100 ns; the second is a conventional amplifier with a peak output pulse proportional to the total ionization as a consequence of the time constants of the pulse shaping circuits, being on the order of a few microseconds [Gi53]. The ratio of pulses is taken by an analogue pulse-height computer; this ratio is proportional to the radial specific ionization of the event and is large for a proton-recoil pulse and considerably smaller, on the average, for an electron-induced pulse of gamma origin. The pulse height distribution of the divider circuit output shows well-separated gamma and proton peaks with energy-independent positions (Fig. 11).

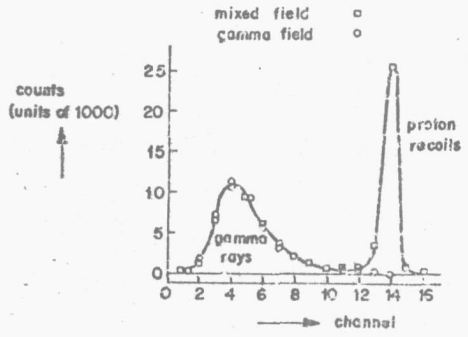

Fig. 11. Output pulse height distribution of divider circuit used by Bennett [Be67].

Rejection of gamma pulses is obtained by using a discriminator circuit with threshold positioned in the "valley" between proton and gamma peak; the discriminator output controls a linear gate circuit between the amplifier giving the energy information and the analog-digital converter of the analyser system.

Because the construction of a fast and accurate analogue pulse height divider is rather complicated [St65]

two other possibilities have been investigated.

The first one involves the measurements of the time interval between start and zero-crossing of the detector pulse after double differentiation with time constants which must be shorter than the rise times of the gamma pulses [So67,Gr69,Ro64]. In practice the usefulness of this technique appeared to be rather limited; the short time constants needed in order to obtain sufficient sensitivity to differences in pulse rise times, give rise to unfavourable signal-to-noise ratios and hence a deterioration of neutron-gamma separation.

Therefore in our laboratory a method has been developed which requires rather simple electronics but in essence gives the same results as the method based on the use of a pulse-height divider. A simplified block diagram of the electronic circuitry is shown in Fig.12.

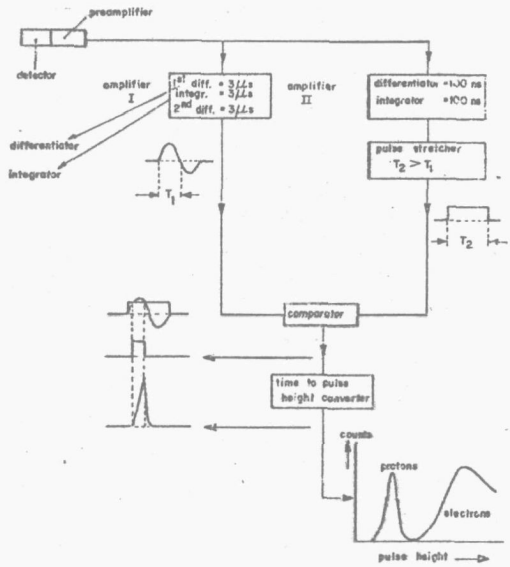

Fig. 12. Block diagram of electronic circuitry for pulse shape discrimination.

In order to preserve the original detector pulse shape and to maximize signal-to-noise ratios, the detector is immediately attached to a low-noise wide-band

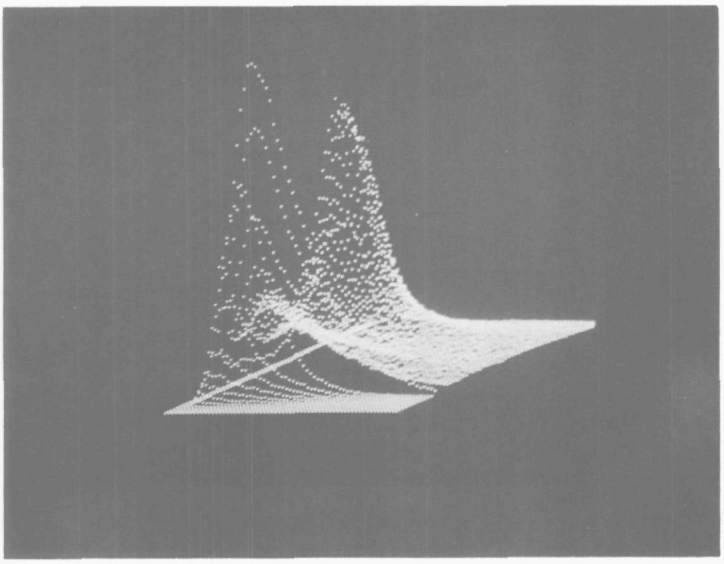

Fig. 13a. Isomeric display of two-parameter spectrum, measured in FANCY (total ionization on horizontal axis).

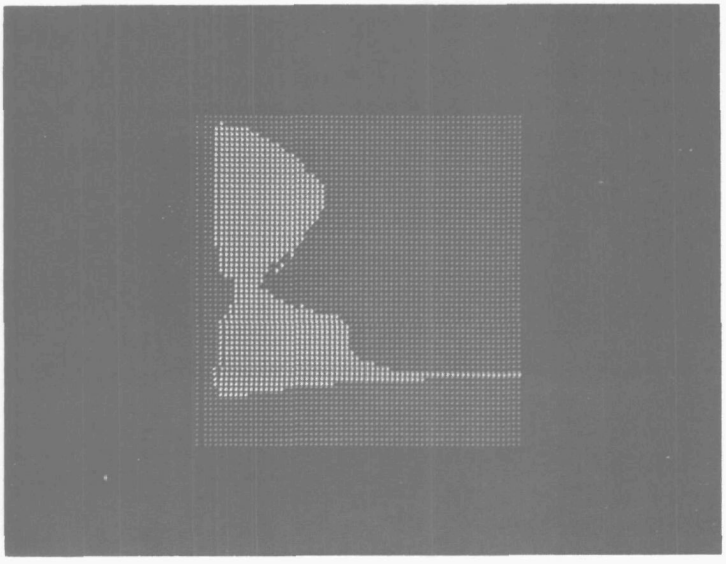

Fig. 13b. Contour display of spectrum shown in figure 13a.
horizontal axis: total ionization.
vertical axis: output pulse height of time-to-pulse height converter of pulse shape discrimination circuit.

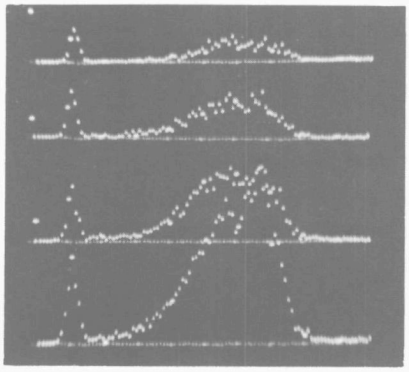

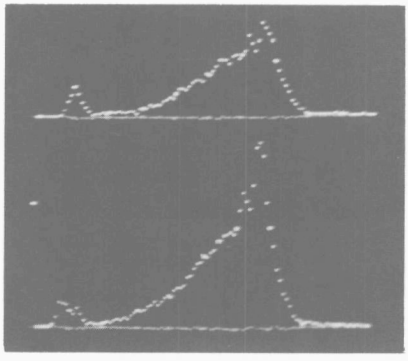

Fig. 14a:

Output spectra of time-to-pulseheight converter of pulse shape discrimination circuit, coincident with total ionization intervals of (from the top downwards):

20 - 25 keV
15 - 20 keV
10 - 15 keV
5 - 10 keV
5 - 7.5 keV
2.5- 5 keV

(measured in FANCY; note increasing gamma-to-neutron ratio with decreasing total ionization)

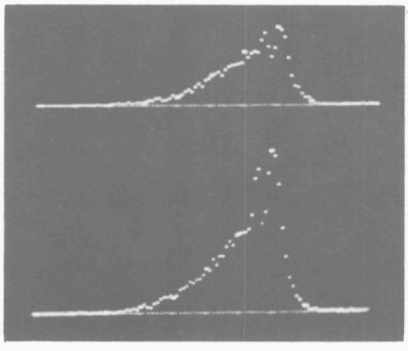

Fig. 14b:

Idem for gamma rays of a ^{60}Co source. Total ionization intervals:

5 - 7.5 keV
2.5- 5 keV

preamplifier with field-effect transistor input [Ra65]. The preamplifier output pulses are amplified and shaped in two channels. The first one consists of a double-differentiating amplifier with time constants long compared to the rise times of the input pulses. In order to prevent the occurence of long pulse "tails" in case of strong overloads, which frequently occur during measurements of the low energy part of the neutron spectrum, pole-zero cancellation is applied [No65,La68]. The amplitudes of the output pulses of this amplifier are proportional to the total energy deposited in the sensitive volume of the detector by a recoil proton or conversion electron. The second channel contains an amplifier with a differentiating time constant which is short compared to the rise time of the gamma pulses. The output pulses of this amplifier are fed to a fast pulse stretcher which produces rectangular pulses of fixed width and with heights proportional to the amplitudes of the input pulses. In order to eliminate baseline shift at high count rates, these pulses are fed into a baseline restorer [Wi68]. The pulses from both channels are presented to the inputs A and B of a comparator circuit, which delivers a rectangular output pulse with a duration equal to the length of the time interval during which the bipolar pulse exceeds the pulse from the baseline restorer. Time-to-pulse-height conversion is obtained by integration of the output pulse of the comparator. As the shapes of the pulses at the inputs A and B are independent of the pulse amplitudes, the output pulse of the time-to-pulse-height converter has an unique relation to the ratio of the pulse amplitudes at A and B. The neutron peak in the output pulse spectrum is positioned at the left side of the gamma peak. For optimum results the amplification factors in both channels must be adjusted in such a way, that the amplitudes of the pulses at A and B are about equal for very short rise time of the detector pulse; in that case maximum sensitivity to rise-time variations in the "valley" region is obtained, because the bipolar pulses at A are rather flat-topped. Further processing of the signals is analogous to Bennett's method described before in this paragraph.

In Figs. 13 and 14 some output spectra of the pulse-shape discrimination circuit are shown. The first figure shows an isomeric display and a contour display

of a two-parameter spectrum (number of counts as a function of both total ionization and "specific ionization") where the valley between the gamma and neutron hills runs parallel to the energy axis; in the second figure output spectra of the pulse-shape discrimination circuit are shown for some energy intervals, both for the spectrum in FANCY and the spectrum of a ^{60}Co source.

III THE NEUTRON TRANSPORT EQUATION

III.1 Introduction

In this Chapter the neutron transport equation is analyzed in some detail. In order to simplify the equations without loss of significant aspects, a non-multiplying medium with a slab geometry will be considered.

First the energy-independent case is treated; this so-called one-group theory may be applied, if the energy distribution of the neutrons considered is space independent.

The next step is the extension to the multigroup treatment which involves a transformation of the energy-dependent transport equation into a set of coupled one-group equations by means of discretization of the energy variable in the form of energy groups. This method is applicable provided the spectrum within each energy group is either not or only slightly space dependent; in this approach a proper choice of group widths and related parameters can be important in certain cases, which will be discussed in more detail in the next Chapter.

For both one-group and multigroup case special attention will be given to the treatment of anisotropic scattering of neutrons.

Finally, some important features of the computer codes, developed for this work, will be outlined.

III.2 One-group transport equation

The transport equation for the one-group, one-dimensional plane geometry case reads:

$$\mu \frac{d}{dx} N(x,\mu) + \Sigma_t N(x,\mu) = S(x,\mu) \qquad (3.1)$$

where

x = space coordinate,
μ = cosine of the angle between the coordinate axis and the direction of the neutron,
$N(x,\mu)$ = flux of neutrons per unit μ-interval about the direction μ at x,

$S(x,\mu)$ = source of neutrons per unit μ-interval about the direction μ at x.

The source term can be written as

$$S(\mu) = \frac{1}{2\pi} \int_0^{2\pi} \int_{-1}^{+1} N(\mu') \Sigma_s(\bar{\mu}) d\mu' d\eta + Q(\mu) \quad , \tag{3.2}$$

where

$\bar{\mu}$ = cosine of the angle between the incident (μ') and emergent directions of a neutron,

η = azimuthal angle between the initial and scattered neutron directions

$$(\bar{\mu} = \mu\mu' + \sqrt{(1-\mu^2)(1-\mu'^2)} \cdot \cos\eta) \quad ,$$

$Q(\mu)$= external (i.e.flux independent) neutron source.

Being not essential for the present discussion of the one-group case, *external* source contributions are further being omitted.

The theoretical basis of the transport equation, especially with respect to anisotropic scattering, is most conveniently illustrated by expanding the flux and the scattering cross section in spherical harmonics of the angular variable [Sn61]:

$$N(\mu) = \sum_{\ell=0}^{\infty} \frac{2\ell+1}{2} \phi_\ell P_\ell(\mu) \quad , \tag{3.3}$$

$$\Sigma_s(\bar{\mu}) = \sum_{\ell=0}^{\infty} \frac{2\ell+1}{2} \Sigma_{s\ell} P_\ell(\bar{\mu}) \quad , \tag{3.4}$$

where the Legendre coefficients are given by:

$$\phi_\ell = \int_{-1}^{+1} N(\mu) P_\ell(\mu) d\mu \quad , \tag{3.5}$$

and

$$\Sigma_{s\ell} = \int_{-1}^{+1} \Sigma_s(\bar{\mu})\, P_\ell(\bar{\mu}) d\bar{\mu} \quad . \tag{3.6}$$

Inserting the Legendre expansions in the expression for the scattering source Eq. (3.2) and using the orthogonality properties of the Legendre functions together with the relation [Sn61]:

$$P_m(\bar{\mu}) = P_m(\mu)P_m(\mu') +$$

$$+ 2 \sum_{n=1}^{m} \frac{(m-n)!}{(m+n)!} P_m^n(\mu)P_m^n(\mu') \cos(n\eta) \quad , \tag{3.7}$$

in which P_m^n are the associated Legendre functions, one obtains:

$$S(\mu) = \sum_{\ell=o}^{\infty} \frac{2\ell+1}{2} \Sigma_{s\ell}\, \phi_\ell\, P_\ell(\mu) = \sum_{\ell=o}^{\infty} \frac{2\ell+1}{2} S_\ell\, P_\ell(\mu) \quad , \tag{3.8}$$

where $S_\ell = \Sigma_{s\ell}\, \phi_\ell$ = the ℓ^{th} spherical harmonic of the scattering source.

One observes that:

$$\phi_o = \int_{-1}^{+1} N(\mu)d\mu = \text{scalar neutron flux},$$

$$\phi_1 = \int_{-1}^{+1} \mu N(\mu)d\mu = \text{net neutron current in the x-direction},$$

whereas

$$\Sigma_{so} = \int_{-1}^{+1} \Sigma_s(\mu)d\mu = \text{total scattering cross section}$$

and

$$\Sigma_{s1} = \int_{-1}^{+1} \mu\Sigma_s(\mu)d\mu = \mu_o \Sigma_{so} \quad , \text{ where } \mu_o \text{ is the mean cosine of the scattering angle.}$$

Substitution of the Legendre expansions into Eq. (3.1) gives:

$$\frac{d}{dx}\left\{ \sum \frac{2\ell+1}{2} \mu\phi_\ell P_\ell(\mu) \right\} + \Sigma_t \sum_\ell \frac{2\ell+1}{2} \phi_\ell P_\ell(\mu) =$$

$$= \sum_\ell \frac{2\ell+1}{2} S_\ell P_\ell(\mu) \quad . \qquad (3.9)$$

Use of the recurrence relation [Sn61]:

$$(m+1) P_{m+1}(\mu) + m P_{m-1}(\mu) = (2m+1) \mu P_m(\mu) \quad , \qquad (3.10)$$

multiplication by $P_m(\mu)$ and integration over the μ-interval of Eq. (3.9) leads to an infinite set of coupled linear differential equations:

$$\frac{d}{dx}\left\{ \frac{m}{2m+1} \phi_{m-1} + \frac{m+1}{2m+1} \phi_{m+1} \right\} + \Sigma_t \phi_m = S_m \quad . \qquad (3.11)$$

From this set a finite system of equations for the so-called P_n approximation of the transport equation is obtained by substituting $\phi_\ell = o$ for $\ell > n$, e.g. for the P_1 approximation:

$$\frac{d\phi_1}{dx} + \Sigma_t \phi_o = \Sigma_s \phi_o \quad , \qquad (3.12)$$

$$\frac{1}{3} \frac{d\phi_o}{dx} + \Sigma_t \phi_1 = \mu_o \Sigma_s \phi_1 \quad . \qquad (3.13)$$

These equations can be reduced to one second-order differential equation:

$$\frac{1}{3\Sigma_{tr}} \frac{d^2\phi_o}{dx^2} + \Sigma_{tr} \phi_o = \Sigma_{str} \phi_o \qquad (3.14)$$

where

$\Sigma_{tr} = \Sigma_t - \mu_o\Sigma_s$ = total transport cross section,

$\Sigma_{str} = \Sigma_s - \mu_o\Sigma_s$ = transport cross section for scattering.

In case of isotropic scattering Eqs. (3.12) and (3.13) lead to the *diffusion equation*:

$$\frac{1}{3\Sigma_t}\frac{d^2\phi_o}{dx} + \Sigma_t\phi_o = \Sigma_s\phi_o \ . \qquad (3.15)$$

Equation (3.14) is often referred to as the *diffusion equation with transport correction*, because by applying corrections to the cross sections in the diffusion equation, anisotropic scattering effects are properly accounted for up to the P_1 component. Physically, the subtraction of the term $\mu_o\Sigma_s$ from both scattering and total cross section means that the angular distribution of scattering is replaced by an isotropic component plus a component leaving the neutron flight direction unaffected (often called delta-forward scattering after the dirac delta function, which in essence means no scattering), such that the mean cosine of scattering angle is the same as in the actual distribution.

Nowadays many computer codes exist based on a more rigorous approximation to the transport equation than the P_1-approcimation (e.g. higher-order P_n codes [Ca62], S_n codes [Du66] and codes based on integral transport theory [Ca68]), but in most cases scattering is handled as being isotropic in order to decrease computer time and memory space required; in those cases the use of *transport corrected cross sections* is recommended. This approach has proven to be a rather good one, e.g. for reactivity calculations [Jo63, Pe62], whereas in this thesis the adequacy of the use of transport corrected cross sections for calculations of space-dependent fast neutron spectra will be analyzed in some detail.

In general an accurate handling of flux anisotropy is more important than a proper treatment of scattering anisotropy, the effect of the latter being of second order; this is due to the fact that the source term on the RHS of Eq. (3.9) contains only an anisotropic

component, if both flux and angular distribution of scattering are anisotropic, which can be seen in Eq. (3.8). This condition is generally met in the higher energy part of the neutron spectrum (above about 1 MeV) where scattering tends to become strongly peaked in the forward direction, which approaches the hypothetical case of delta-forward scattering on which the *transport corrected cross sections* are based.

III.3 Multigroup transport equation

In multigroup theory the continuous energy distribution of neutrons is approximated by introducing a finite number of energy groups with properly defined group cross sections. In this Chapter the groups are numbered (superscript g) beginning at the highest energy group; in the source part of the transport equation a term is added for transfers between groups by elastic and inelastic scattering:

$$\frac{d}{dx}\frac{m}{2m+1}\phi^g_{m-1} + \frac{m+1}{2m+1}\phi^g_{m+1} + \Sigma^g_t \phi^g_m = \sum_{g'} \Sigma^{g'g}_m \phi^{g'}_m \quad . \qquad (3.16)$$

For non-thermal energy groups the right side of the equation contains only terms with $g' \leq g$ because energy gain in scattering processes ("upscattering") is not possible.

For the P_1-approximation one obtains:

$$\frac{d}{dx}\phi^g_1 + \Sigma^g_t \phi^g_o = \sum_{g'} \Sigma^{g'g}_o \phi^{g'}_o \quad , \qquad (3.17)$$

$$\frac{1}{3}\frac{d}{dx}\phi^g_o + \Sigma^g_t \phi^g_1 = \sum_{g'} \Sigma^{g'g}_1 \phi^{g'}_1 \quad . \qquad (3.18)$$

The summation in the second equation is seen to include anisotropic scattering components transferred from other groups. For this reason the use of these multigroup equations is referred to as the *consistent P_1-approximation* [We58].

In the multigroup case the definition of transport corrected cross sections is not as in the one-group case. In order to simplify the notation of the equations, it will be assumed that slowing-down scattering from each energy group extends only to the next lower energy group

(for processes such as inelastic scattering or elastic scattering with light nuclei, which can lead to large energy degradations of the neutrons, the analysis is completely analogous and leads to the same conclusions); in this case the P_1-equations read:

$$\frac{d\phi_1^g}{dx} + \Sigma_t^g \phi_o^g = \Sigma_o^{gg} \phi_o^g + \Sigma_o^{g-1,g} \phi_o^{g-1} \quad , \tag{3.19}$$

$$\frac{1}{3} \frac{d\phi_o^g}{dx} + \Sigma_t^g \phi_1^g = \Sigma_1^{gg} \phi_1^g + \Sigma_1^{g-1,g} \phi_1^{g-1} \quad . \tag{3.20}$$

Equation (3.20) can be rewritten as:

$$\phi_1^g = - \frac{1}{3(\Sigma_t^g - \Sigma_1^{gg} - \Sigma_1^{g-1,g} \frac{\phi_1^{g-1}}{\phi_1^g})} \frac{d\phi_o^g}{dx} \quad . \tag{3.21}$$

Equations (3.19 and (3.20) can be reduced to one second-order equation for the scalar flux ϕ_o^g by adopting either of the next approximations:

a. $\Sigma_1^{g-1,g} \phi_1^{g-1} = o$, i.e. the anisotropic slowing-down source is neglected;

b. $\Sigma_1^{g-1,g} \phi_1^{g-1} = \Sigma_1^{g,g+1} \phi_1^g$, i.e. the anisotropic slowing-down source for the group considered is balanced by the anisotropic out-scattering from the group.

In both cases transport corrections are applied only to the cross sections for scattering *within* the groups; for this reason these methods are referred to as *diagonal transport approximations*, because in the matrix of scattering cross sections the *diagonal* elements are modified. The transport cross sections are evaluated according to:

case a: $\Sigma_{tr}^g = \Sigma_t^g - \Sigma_1^{gg}$ (3.22)

$$\Sigma^{g'g}_{str} = \Sigma^{g'g}_{o} - \delta_{g'g} \cdot \Sigma^{g'g}_{1} \qquad (3.23)$$

the so-called *diagonal transport approximation* (DTA) [Ab64].

case b: $$\Sigma^{g}_{tr} = \Sigma^{g}_{t} - \Sigma^{gg}_{1} - \Sigma^{g,g+1}_{1} \qquad (3.24)$$

$$\Sigma^{g'g}_{str} = \Sigma^{g'g}_{o} - \delta_{g'g} \cdot (\Sigma^{gg}_{1} + \Sigma^{g,g+1}_{1}) \qquad (3.25)$$

the so-called *corrected diagonal transport approximation* (CDTA) [Ab64].

In both cases the diffusion equation with transport correction reads:

$$\frac{1}{3\Sigma^{g}_{tr}} \frac{d^2}{dx^2} \phi^{g}_{o} + \Sigma^{g}_{tr} \phi^{g}_{o} = \sum_{g'} \Sigma^{g'g}_{str} \phi^{g'}_{o} \quad . \qquad (3.26)$$

As in the one-group case, the use of *transport cross sections* is recommended in diffusion codes; this also applies to more advanced codes, if the algorithm of these codes is based on isotropic scattering.

In Ref. [Ab64] it is stated that the CDTA method gives more reliable results than the DTA method; an analysis of the physical background of these approximation is lacking however and therefore has been presented above. The statement concerned in Ref. [Ab64] may be based on the fact that assumption b is less approximative than assumption a. In section III.5 the adequacy of DTA and CDTA will be analyze in more detail for the case of a hydrogeneous medium, in which case scattering is strongly anisotropic. It will be shown that the statement in Ref. [Ab64] is not generally true.

An illustration of cross-section values for hydrogen obtained by different approximations is given in Table I for an energy group between 6.5 MeV and 10.5 MeV. For this rather extreme case a negative scattering cross section (physically equivalent to absorption) is obtained in the CDTA case. It may be noted that for physical reasons it is not advisable to apply transport corrections to slowing-down cross sections; in that case the source terms for the lower energy groups would be incorrect. Because the spatial propagation of neutrons is determined by the transport and intragroup scattering

cross sections, the corrections must be restricted to these parameters.

	σ^{1}_{tr}	σ^{11}	σ^{12}	σ^{13}	σ^{14}	σ^{15}
uncorrected cross sections	1.20	0.160	0.400	0.240	0.176	0.096
DTA	1.049	0.009	"	"	"	"
CDTA	0.40	-0.60	"	"	"	"

Table I. Cross sections for hydrogen with different transport approximations (6.5 MeV-10.5 MeV).

III.4 Computer codes for spectrum calculations

Three basicly different ALGOL computer codes have been developed for the numerical solution of the transport equation:

1. the one-dimensional diffusion code FAST-ZOOM-DELFT [Da67];
2. the one-dimensional S_N-code FAST-DSN-DELFT. Two versions of this code exist, an isotropic and an anisotropic scattering version [Br69];
3. the two-dimensional S_N-code XYSNI [Ho70];

the first code solves the one-dimensional multigroup transport equations in diffusion approximation, preferably with *transport corrected cross sections* as input. Limitations in the applicability of this code are posed by the fact that in the diffusion approximation all second and higher Legendre components of the differential neutron flux are neglected. Therefore the diffusion approximation is expected to be rather poor in case of strongly anisotropic neutron fields i.e. with strong flux gradients as for instance exist in systems with small dimensions or in regions near boundaries or external sources.

In order to understand the differences between the results of respectively diffusion calculations and more exact calculations it is useful to analyse the diffusion approximation in some detail.

The exact one-dimensional transport equation in

plane geometry reads:

$$\frac{d\phi_1}{dx} + \Sigma_a \phi_o = S_o \quad . \tag{3.27}$$

The approximative character of all transport calculations is based on the treatment of the net leakage term $\frac{d\phi_1}{dx}$.

From Eq. (3.11) the following expressions for ϕ_1 can be obtained for the case of isotropic scattering:

diffusion approximations: $$\phi_1 = -\frac{1}{3\Sigma_{tr}} \frac{d\phi_o}{dx} \tag{3.28}$$

exact: $$\phi_1 = -\frac{1}{3\Sigma_{tr}} \frac{d}{dx} (\phi_o + 2\phi_2) \quad . \tag{3.29}$$

The influence of the component ϕ_2 can be assessed from the P_2-approximation:

$$\phi_2 = -\frac{2}{5\Sigma_{tr}} \frac{d\phi_1}{dx} \quad . \tag{3.30}$$

It can be easily seen that in the case of positive net leakage (i.e. the external source exceeds the absorption rate of neutrons) the neutron current will be overestimated by diffusion theory; this is consistent with the fact that the critical size of reactor cores is overestimated in diffusion calculations [Ok55]. In case of negative net leakage, for instance in absorbing regions without external sources, the opposite is true. As a consequence the flux level near an external source is underestimated by diffusion theory whereas at distances greater than a few mean free paths the flux is overestimated. In the case of a non-multiplying medium fed by an external fast neutron source the spectrum near the source as calculated with diffusion theory is too soft because of an underestimation of the flux of unmoderated neutrons and a relative overestimation of the flux of moderated neutrons for which the source, due to slowing down, is more spatially distributed. Similar analysis gives too hard diffusion-

theory spectra at greater distances from the source.

In order to obtain a better approximation for the solution of the transport equation more detailed calculations of the angular dependence of the neutron flux are required. For this purpose the S_N-method of Carlson has been adopted [Ca55, Ca59, Ca 60, Le62] based on discretization of the angular dependence of the neutron flux (the index N refers to the number of discrete angular directions). For a detailed description the reader is referred to the computer code reports [Br69, Ho70].

The one-dimensional codes have been used for calculations on FANCY-cores that could be approximated as having spherical symmetry. The two-dimensional code was used for calculations on cores with approximately cylindrical symmetry, e.g. cores with measuring channels or symmetrically inserted elements with compositions differing from the core material.

To study the influence of scattering anisotropy on the space and energy-dependent neutron distribution, the one-dimensional S_N-code in anisotropic scattering version has been used. In this code, the Legendre components of the scattering cross sections up to the P_4 components must be supplied as part of the input. The evaluation of anisotropic source terms in this code is based on a theory, developed in [Pe62].

Finally, some remarks concerning the use of diffusion codes versus the use of more sophisticated transport codes can be made here. For systems with small flux gradients the use of a diffusion code must be preferred because of the high computation speed and sufficient accuracy. In case of systems which require the application of transport codes (e.g. because of strong flux anisotropy) it is useful to consider the inaccuracies caused by uncertainties in group cross-section values. In some cases the cross-section behaviour *per se* may be accurately known but the use of rather broad energy groups may cause doubts about the proper values of group parameters. In that case a 26-group diffusion calculation may give better results and require less computation time than a 14-group S_4-calculation.

III.5 The adequacy of the use of transport cross sections for a hydrogeneous medium

In order to determine the adequacy of the use of cross sections with different transport approximations, some calculations using the anisotropic scattering version of the code FAST-DSN-DELFT [Br69] have been performed on a system which is rather extreme from the view-point of anisotropic scattering effects. The relevant data of this testcase are:

geometry of the system:	sphere with 50 cm. radius
geometry of the source:	spherical shell extending from r=5 cm. to r=6 cm.
number of energy groups:	2 (6.5 MeV - 10.5 MeV resp. 4.0 MeV - 6.5 MeV)
source spectrum and source strength:	the same number of neutrons (1 $n.cm^{-3}.s^{-1}$) is emitted in each energy group
material composition:	hydrogen with a nuclear density of 0.0833 10^{24} cm^{-3}.
cross section values and angular scattering distribution data:	taken from the ABN-set [Ab64], energy groups 6.5 - 10.5 MeV and 4.0 - 6.5 MeV.

As a consequence of the material composition and the geometry of this system (small source in the centre of a large sphere), the transport of neutrons is strongly influenced by the scattering anisotropy. In Table II results are presented of calculations with different methods for treatment of anisotropic scattering. The data refer to the flux in the centre of the assembly and the neutron leakage at the assembly boundary; it is obvious that the values obtained for the last quantity are very sensitive to the calculation method applied.

The results of Table II indicate good accuracy for the DTA method, whereas the CDTA method gives a considerable overestimation of the neutron leakage together with an underestimation of the centre flux.

The accuracy of the DTA method for the highest energy group can be understood on the basis of the analysis, presented in section III.3, because there is

method:	group:	centre flux ($n.cm^{-2}.s^{-1}$):	leakage (%)
P_o	1	0.6616	0.615
	2	0.7471	0.230
P_1	1	0.6308	0.842
	2	0.7021	0.348
P_2	1	0.6393	0.883
	2	0.7100	0.370
P_3	1	0.6352	0.893
	2	0.7063	0.375
P_4	1	0.6466	0.898
	2	0.7250	0.377
DTA	1	0.6384	0.880
	2	0.7101	0.380
CDTA	1	0.5328	4.355
	2	0.5770	2.415
MDTA	1	0.6384	0.880
	2	0.6659	0.712

Table II. Results of calculations on a spherical hydrogen assembly (S_4 calculations).

P_n : angular distribution of scattering is treated exact up to the P_{n+1} component.

DTA : diagonal transport approximation.

CDTA : corrected diagonal transport approximation.

MDTA : modified diagonal transport approximation.

no anisotropic slowing- down source for this group. The MDTA-method is based on the use of a transport cross section consistent with Eq. (3.21):

$$\Sigma_{tr}^{g} = \Sigma_{t}^{g} - \Sigma_{1}^{gg} - \Sigma_{1}^{g-1,g} \frac{\phi_{1}^{g-1}}{\phi_{1}^{g}} \qquad (3.31)$$

Since the ratio of the neutron currents appears on the RHS of the equation, the transport cross section will be generally space-dependent in the MDTA-scheme. This approach was first published by Rakavy and Yeivin [Ra63], and has been applied for instance in Ref. [Fi70]. It can be shown that this approach is better than the DTA-method provided the second and higher Legendre components of the angular flux can be neglected a condition which is obviously not fulfilled for the system studied above, where the flux is strongly peaked in the radial direction.

For the calculations the Legendre components of the scattering cross sections must be supplied as part of the input. For the particular case of hydrogen these components can be obtained as follows. The cross section $\sigma^{jk}(\mu)$ for neutron scattering from group j to group k as a function of μ(cosine of scattering angle) can be approximated as:

$$\sigma^{jk}(\mu) = \sigma^{jk} \cdot \delta(\mu - \bar{\mu}_{jk}) \qquad (3.31)$$

where δ = Dirac delta function
$\bar{\mu}_{jk}$ = mean cosine of scattering angle for transfer from group j to group k

because the spreading of the scattering angle for a particular group-to-group transfer is rather small as a consequence of the approximately equal masses of neutron and hydrogen nucleus. The Legendre components are then evaluated according to Eq. (3.6):

$$\sigma_{\ell}^{jk} = \int_{-1}^{+1} \sigma^{jk}(\mu) P_{\ell}(\mu) d\mu =$$

$$= \sigma^{jk} \int_{-1}^{+1} \delta\,(\mu - \bar{\mu}_{jk}) P_\ell(\mu)\,d\mu = \sigma^{jk} \cdot P_\ell(\bar{\mu}_{jk}) \quad . \tag{3.32}$$

In Fig. 15 the different Legendre approximations, obtained with this technique for the angular dependence of hydrogen slowing-down scattering are shown for $\bar{\mu}_{jk} = 0.8$. The latter value is related to scattering from ABN-group 3 (2.5 MeV - 4 MeV) to group 4 (1.4 MeV - 2.5 MeV) [Ab64]. The curve designated as "actual distribution" must be considered as being approximative, because of its dependence on the intragroup spectrum.

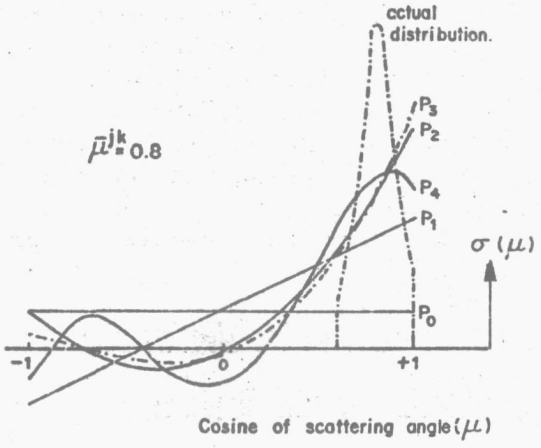

Fig. 15. Approximations of the angular dependence of the slowing-down cross section of hydrogen with different Legendre expansions.

IV GROUP CROSS SECTIONS *)

IV.1 Introduction

In this Chapter an analysis is given of the evaluation of group cross sections to be used as parameters in diffusion and transport calculations. First a survey is given of the consequences arising from the discretization of the energy variable in multigroup calculations; definitions of group cross sections are obtained by imposing the condition that discretized and non-discretized forms of the transport equation must be equivalent. From these considerations it is concluded that in almost all practical cases only approximate values of group parameters can be evaluated.

In section IV.3 an analysis is presented of group cross section evaluation in case of cross section resonance effects and associated resonance self-shielding; the mutual interference of group cross sections for a mixture of a resonance scatterer and a potential scatterer is demonstrated.

In the last section of this Chapter the influence of neutron leakage on group cross section values is discussed; finally a method is presented which can be used either for increasing the accuracy of calculations on space-dependent energy distributions or for the procurement of group cross sections from measured spectra.

IV.2 Group cross section definitions

IV.2.1 Diffusion approximation

The energy-dependent diffusion equation reads:

$$D(r,E)\nabla^2\phi(r,E) - \Sigma_{rem}(r,E)\phi(r,E) + Q(r,E) = o \qquad (4.1)$$

where

D = $1/3\ \Sigma_{tr}$ = diffusion coefficient
Σ_{tr} = transport cross section, as defined in Chapter III,
Σ_{rem} = removal cross section, both for absorption and energy degradation,
Q = source term, taking external sources and moderation into account.

*) This Chapter was partially published earlier in Ref. [Da68].

Integration of Eq. (4.1) over an energy interval g leads to a *group equation*:

$$D^g(r)\nabla^2\phi^g(r) - \Sigma^g_{rem}(r)\phi^g(r) + Q^g(r) = o \qquad (4.2)$$

where

$$\phi^g(r) = \text{group flux} = \int_g \phi(r,E)dE \ .$$

Definitions for the group parameters are obtained by applying the equivalence condition for Eqs. (4.1) and (4.2):

$$D^g(r) = \int_g D(r,E)\nabla^2\phi(r,E)dE \ / \ \int_g \nabla^2\phi(r,E)dE \qquad (4.3)$$

$$\Sigma^g_{rem}(r) = \int_g \Sigma'_{rem}(r,E)\phi(r,E)dE \ / \ \int_g \phi(r,E)dE \qquad (4.4)$$

$$Q^g(r) = \int_g Q'(r,E)dE \ , \qquad (4.5)$$

where $\Sigma'_{rem}(r,E)$ denotes the removal cross section, taking into account only absorption and energy degradation removing the neutrons from the group g; analogously $Q'(r,E)$ denotes the source term for external sources and neutrons moderated from higher energy groups, i.e. the intragroup scattering components of $\Sigma_{rem}(r,E)$ and $Q(r,E)$ are eliminated.

From these equations it is concluded that group parameters in general depend on the intragroup spectrum. In addition it may be concluded that group cross sections are space-*in*dependent only if the spectrum is space-independent, which means energy-space separability of the flux $\phi(r,E)$. In the latter case Eq. (4.3) may be rewritten as:

$$D^g = \int_g D(E)\phi(E)dE \ / \ \phi^g \ . \qquad (4.6)$$

Because in general the group diffusion coefficient is calculated from the transport cross section, the correct value for the group transport cross section is obtained by taking the reciprocal of the flux-weighed average of $1/\Sigma_{tr}(E)$, which in case of space-energy separability is equivalent to the current-weighed average of $\Sigma_{tr}(E)$:

$$\Sigma^g_{tr} = \int_g \phi(E)dE \Big/ \int_g \frac{\phi(E)}{\Sigma_{tr}(E)} dE =$$

$$= \int_g \Sigma_{tr}(E)J(E)dE \Big/ \int_g J(E)dE \ . \qquad (4.7)$$

An important difference may be noted:

a. the evaluation of the group transport cross section is based on conservation of neutron current
b. the evaluation of other group parameters is based in conservation of reaction rate.

IV.2.2 Transport calculations

For transport calculations, such as S_N, a more detailed analysis of the group cross-section evaluation is required.

The one-dimensional transport equation in plane geometry reads:

$$\mu \frac{\partial}{\partial x} N(x,E,\mu) + \Sigma_t(x,E)N(x,E,\mu) =$$

$$= \sum_{n=o}^{\infty} \frac{2n+1}{2} P_n(\mu) \int \phi_n(x,E') \times$$

$$\times \Sigma_n(E' \to E,x)dE' + S(x,E,\mu) \qquad (4.8)$$

where

$$N(x,E,\mu) = \sum_n \frac{2n+1}{2} P_n(\mu)\ \phi_n(x,E) \ . \qquad (4.9)$$

Integration over an energy interval g leads to:

$$\mu \frac{\partial}{\partial x} N^g(x,\mu) + \sum_n \frac{2n+1}{2} P_n(\mu) \cdot \Sigma_t^g(n,x) \cdot \phi_n^g(x) =$$

$$= \sum_n \frac{2n+1}{2} P_n(\mu) \sum_{g'} \Sigma_n^{g'g}(n,x) \phi_n^{g'}(x) + S^g(x,\mu) \tag{4.10}$$

where

$$\phi_n^g(x) = \int_g \phi_n(x,E)dE \tag{4.11}$$

$$\Sigma_t^g(n,x) = \int_g \Sigma_t(x,E) \phi_n(x,E)dE \; / \; \phi_n^g(x) \tag{4.12}$$

$$\Sigma_n^{g'g}(n,x) = \int_{g'} \phi_n(x,E')dE' \int_g \Sigma_n(E' \to E,x)dE \; / \; \phi_n^{g'}(x) \; . \tag{4.13}$$

Rearranging terms and considering intragroup interactions only gives:

$$\mu \frac{\partial}{\partial x} N^g(x,\mu) +$$

$$+ \sum_n \frac{2n+1}{2} P_n(\mu) \left\{ \Sigma_t^g(n,x) - \Sigma_n^{gg}(n,x) \right\} \phi_n^g(x) = \; . \; . \tag{4.14}$$

In general the group cross sections will be both space- and angle-dependent. In actual calculations it is, however, convenient to use angle-independent total cross sections which give the best approximation to Eq. (4.10); in this case Eq. (4.10) is approximated by:

$$\mu \frac{\partial}{\partial x} N^g(x,\mu) + \Sigma_t^g(x) \sum_n \frac{2n+1}{2} P_n(\mu) \phi_n^g(x) =$$

$$= \sum_n \frac{2n+1}{2} P_n(\mu) \Sigma_n^{gg}(x) \phi_n^g(x) + \; . \; . \; . \; . \tag{4.15}$$

and in order to fulfil the condition of conservation of neutron current:

$$\Sigma_t^g(x) = \Sigma_t^g(1,x) = \int \Sigma_t(E,x) \phi_1(E,x)dE \; / \int \phi_1(E,x)dE \tag{4.16}$$

which is analogous to Eq. (4.7) for the diffusion approximation.

In order to have conservation of removal (absorption + moderation) from the group the cross section $\Sigma_o^{gg}(o,x)$ must be chosen according to

$$\Sigma_t^g(x) - \Sigma_o^{gg}(o,x) = \Sigma_{rem}^g(x) \qquad (4.17)$$

where Σ_{rem}^g is calculated according to Eq. (4.4).

It can be concluded that the same group cross-section definitions apply to both transport and diffusion calculations; the intragroup scattering cross section, which appears explicitly in the transport equations only, is obtained by taking the difference between total (or transport) cross section and removal cross section.

It may be noted that in case of multigroup transport calculations the group cross-section set to be used is generally obtained by averaging methods which are based on less rigorous transport equations.

IV.2.3 Final remarks

It is clear from the analysis in the preceding paragraphs that a group cross-section set is based on a well-defined averaging spectrum and can be used only for calculations on systems with a neutron spectrum not deviating strongly from the averaging spectrum; therefore care must be taken, when using one of the standard cross-section sets.

Obviously the sensitivity of a group cross-section set to the averaging spectrum decreases when the number of energy groups is increased. In practice the number of energy groups and space points that can be used in calculations on fast systems depends on the computer capacity. At present space-dependent spectrum calculations are performed with some 10 to 30 energy groups. As a consequence an accurate evaluation of group parameters is necessary but mostly rather difficult. In case of large multiplying systems this evaluation can be based on space-independent fundamental mode calculations with a large number of groups, say 100 to 1000, such as ELMOE and MC2 [Ra64,To67]; these calculations are based on energy-space separability of neutron flux, which assumption is adequate for the central part of large cores but fails near core-reflector interfaces,

where the group parameters have to be adjusted [Me66]. For systems with strongly space-dependent spectra a general solution cannot be given.

The problems associated with the evaluation of cross-section sets can be illustrated by some of the results of a comparison between measured parameters of a plutonium fueled zero-energy assembly (ZPR-3 assembly 48) and those calculated independently by 11 members of an international group of establishments which are active in the field of fast reactors [Da66]:

1. calculated critical masses deviate from -23% to +15% from the measured critical mass,
2. the calculated flux fractions below resp. 9.1 keV and 1.23 keV, which play an important role in connection to Doppler effects, show a spreading of respectively ±17% and ±33%,
3. calculated Doppler effects for U^{238} differed from +36% to -25% from the measured effect; the corresponding figures for Pu^{239} are ranging from +145% to +700%.

In a recent study of a dilute plutonium-fueled assembly [Fi70] the next results are obtained:

1. calculated values for k_{eff} differ from -4.9% to +2,65% from the measured k_{eff}, depending on the cross-section set used,
2. predicted coolant reactivity coefficients deviate -26% to +14% from measured values,
3. fission rate ratios of ^{238}U and ^{239}Pu relative to ^{235}U are underpredicted by resp. 19% and 11%.

In Ref. [Wa68] data are presented how accurately the information concerning the neutronic behaviour of fast reactors should be known in the future; the so-called target design accuracies of the quantities mentioned above are respectively 1%, 10% and 2% whereas the present accuracy of the calculated quantities is estimated to be ≥ 3%, 50% and 20%.

IV.3 Group cross sections for resonance scattering materials

IV.3.1 Introduction

In this section the evaluation of group cross sections for media containing resonance scattering

nuclides is presented in more detail. In practice this situation is always encountered because of the presence of structural materials such as iron, chromium, nickel or, like in some experimental cores, aluminium; these materials show many pronounced scattering resonances in the energy region from a few keV upto about 500 keV (fig. 16).

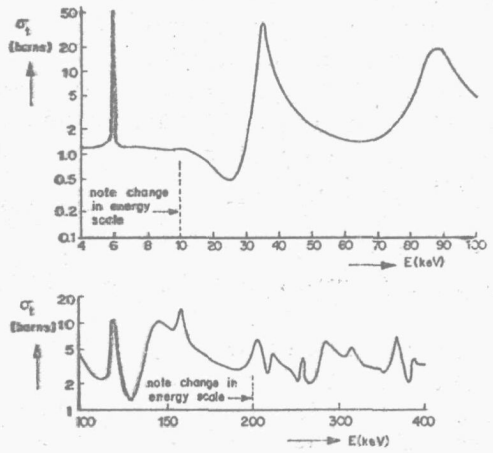

Fig. 16. Total cross section of aluminium in the energy region from 10 keV to 400 keV (Ref. [St64]).

These resonances introduce flux depressions at resonance energies and sometimes strong flux enhancements due to cross-section minima caused by the interference of resonance and potential scattering [We58]. The intragroup spectrum $\phi(E)$ is determined by the cross-section behaviour of all nuclides present in the medium; as a consequence the group cross-section for a certain nuclide is in general composition-dependent. A rather strong dependence exists when cross-section resonances are present within the group considered or in those parts of higher energy groups which contribute to the group flux by neutrons which have suffered less than about three slowing-down collisions.

Although these considerations are generally recognized, in many cases use is made of group cross-sections obtained by simple homogenization of data from cross-section sets. Therefore a study of the adequacy of this procedure was felt to be useful. In order to be more

specific, the cases have been studied of pure aluminium (e.g. the FANCY core) and a mixture of aluminium and graphite; the last case is interesting with regard to the interference between group cross sections of different nuclides and the analysis of the spectral behaviour near the aluminium-graphite interface of FANCY.

The group structure (energy interval spreading) of the Russian ABN-set [Ab64] has been adopted and calculated group constants will be shown for the four groups between 21.5 keV and 400 keV, containing many aluminium scattering resonances, the most important ones at resp. 35 keV and 88 keV. Between 21.5 keV and 400 keV the total carbon cross section decreases smoothly from 4.64 barn to 3.60 barn.

The contributions of resonances to a group cross section are diminished due to the decreased flux magnitudes at the resonance energies, an effect known as self-shielding. This self-shielding decreases with increasing admixture of non-resonant nuclides and is absent in the asymptotic case of infinite dilution because of the resulting smooth energy dependence of the flux. In the case of aluminium and graphite only the scattering cross sections have to be considered because absorption can be neglected. The graphite microscopic group cross section for total scattering can be taken independent of the mixing ratio because the graphite cross section is approximately energy-independent. For aluminium self-shielding of the total scattering cross section is evident. For both materials the cross section for neutron transfer to a lower energy group due to elastic moderation is expected to be rather sensitive to the mixing ratio; inelastic scattering is absent in the energy range considered. Only those neutrons with an energy near the lower boundary of the group can contribute to the moderation and therefore the slowing-down cross section is a function of the ratio of the flux in the moderation interval to the total group flux. Clearly the positions of resonances relative to the boundaries of the group interval are important in the evaluation of the transfer of neutrons out of the interval.

IV.3.2 Calculation methode

For determining the group constants a calculation

of intragroup spectra $\phi(E)$ is required. The results reported here are based on the assumption of an infinitely large system whereas in the energy range considered the contribution of first-flight source neutrons is negligible; these assumptions are not essential but provide a good reference case. Three methods to determine intragroup spectra, based on different assumptions to be discussed, can be adopted:

$$\text{method A:} \quad F(E) :: \frac{1}{E} \tag{4.18}$$

$$\text{method B:} \quad F(E) :: 1 \,/\, \bar{\xi}(E)E \tag{4.19}$$

$$\text{method C:} \quad F(E) = \int_{E}^{E/\alpha^{c}} \frac{F^{c}(E')}{E'(1-\alpha^{c})}\, dE' + \int_{E}^{E/\alpha^{al}} \frac{F^{al}(E')}{E'(1-\alpha^{al})}\, dE' \tag{4.20}$$

where

$F(E)$ = collision density = $\Sigma_t(E)\phi(E)$, in our case equal to $\Sigma_s(E)\phi(E)$,
$\bar{\xi}(E)$ = mean logarithmic energy decrement per scattering event for the mixture,
$1-\alpha$ = maximum fractional energy decrease per elastic collision,

superscripts: c = graphite, al = aluminium.

Method A is valid for a small resonance width compared to the mean energy loss of neutrons per collision, method B is suitable for very broad resonances whereas method C is exact.

Table I shows some data, obtained from [St64], for two resonances of aluminium from which it can be concluded that both resonances can be considered intermediate cases between narrow and broad.

In order to evaluate group cross sections numerical calculations were performed based on Eqs. (4.18), (4.19) and (4.20); the energy range from 20 keV to 500 keV was divided into 480 energy groups with equal energy width

whereas the cross section curve was approximated by step functions.

resonance energy E_o (keV)	$\Gamma_t \simeq \Gamma_n$ (keV)	$E_o.\xi^{al}(E_o)$ (keV)	$E_o.\xi^{c}(E_o)$ (keV)
35	4	2.5	5.5
88	11	6	14

Table I. Widths of aluminium resonances and mean energy losses associated with elastic collisions.

The slowing-down cross section for both materials has been found by calculating the number of slowing-down collisions for each nuclide and dividing by the product of group flux and nuclide concentration. The total group cross section of aluminium was evaluated according to:

$$\Sigma_t^{al} = \frac{\int_g \frac{\Sigma_t^{al}(E)}{\Sigma_t^{al}(E)+\Sigma_t^{c}} \phi(E)dE}{\int_g \frac{\phi(E)}{\Sigma_t^{al}(E)+\Sigma_t^{c}} dE} \qquad (4.21)$$

which is connected with Eq. (4.7): by using this definition, the total cross section for the mixture is obtained by simple homogenization of the cross sections of the components.

IV. 3.3. Results and Discussion

Table II shows the results for the total cross section σ_t and slowing-down cross section σ_d of aluminium and graphite. The parameter σ_o denotes the graphite scattering cross section per aluminium atom in barns; σ_o = 10 barns corresponds with an atom mixing ratio of C: Al = 2.2 and a volume mixing ratio of 1.65. For comparison the corresponding ABN values are given between brackets. Due to the limited accuracy of the microscopic data used and the approximations introduced as a consequence of the discretization of all variables used in the numerical code, not all decimals can be considered as significant.

		σ_o = 0 b.			σ_o = 1 b.			σ_o = 10 b.			σ_o = 100 b.			σ_o = 1000 b.		
group	method	σ_t^{Al}	σ_d^{Al}	σ_d^{C}	σ_t^{Al}	σ_d^{Al}	σ_d^{C}	σ_t^{Al}	σ_d^{Al}	σ_d^{C}	σ_t^{Al}	σ_d^{Al}	σ_d^{C}	σ_t^{Al}	σ_d^{Al}	σ_d^{C}
7	A	3.24	0.358		3.34	0.382	0.856	3.64	0.455	0.880	3.79	0.493	0.892	3.82	0.501	0.900
	B	3.24	0.358		3.34	0.404	0.864	3.64	0.476	0.890	3.80	0.497	0.892	3.82	0.502	0.896
200-400 keV	C	3.24	0.358		3.34	0.385	0.852	3.64	0.458	0.876	3.80	0.495	0.892	3.82	0.502	0.896
	ABN	2.65	0.312		2.96	0.326		3.28	0.356					3.90	0.371	0.899
8	A	2.64	0.346		2.98	0.355	1.148	3.97	0.347	1.041	4.77	0.326	0.968	4.92	0.321	0.955
	B	2.64	0.346		3.11	0.357	1.122	4.15	0.338	1.002	4.81	0.322	0.967	4.92	0.321	0.955
100-200 keV	C	2.64	0.346		2.98	0.335	1.097	4.00	0.332	0.962	4.78	0.323	0.976	4.92	0.321	0.955
	ABN	2.56	0.371		3.07	0.397		4.21	0.471					5.20	0.523	0.972
9	A	1.82	0.228		1.98	0.244	1.107	2.86	0.248	1.035	4.20	0.232	0.945	4.55	0.227	0.929
	B	1.82	0.228		2.06	0.251	1.102	3.11	0.241	0.994	4.30	0.228	0.934	4.56	0.228	0.924
46.5-100 keV	C	1.82	0.228		2.04	0.237	1.044	3.03	0.237	0.976	4.26	0.228	0.934	4.56	0.228	0.924
	ABN	1.85	0.239		2.05	0.262	0.923	3.15	0.359	0.923			0.923	5.00	0.460	0.923
10	A	0.611	0.121		0.881	0.099	1.75	2.41	0.070	1.242	5.23	0.056	1.003	6.31	0.053	0.957
	B	0.611	0.121		1.01	0.088	1.57	2.84	0.063	1.122	5.52	0.055	0.980	6.35	0.053	0.954
21.5-46.5 keV	C	0.611	0.122		0.996	0.084	1.52	2.71	0.063	1.113	5.39	0.055	0.980	6.33	0.054	0.954
	ABN	0.74	0.137		1.04	0.213	0.944	2.96	0.419	0.944			0.944	7.40	0.687	0.944

Table II. Group cross sections for aluminium and graphite as a function of mixing ratio.

The "infinite dilute" values ($\sigma_o = 10^3$ barns) for $\langle\sigma_t\rangle$ of aluminium are about 10% lower than those given by ABN. This is due to the use of newer data for aluminium cross sections (compare Ref. [Hi59] and [Ga64]); further it can be seen that self-shielding with decreasing σ_o is not so strong as indicated by ABN. Method A gives a stronger flux depression in resonance regions than method B as might be expected. Method C gives intermediate values and must be used in cases with small σ_o and/or strong resonances.

The values for the slowing-down cross section of aluminium show rather large discrepancies when compared to the ABN-values. The ABN-values are much too large which is caused by the calculation method used in the ABN-set (which is correct only if the elastic scattering cross section is energy-independent);

$$\langle\sigma_d\rangle = \frac{\xi}{\Delta u} \cdot \langle\sigma_e\rangle \qquad (4.22)$$

where

$\langle\sigma_d\rangle$ = group cross section for slowing-down,
Δu = group width in lethargy units,
$\langle\sigma_e\rangle$ = group cross section for elastic scattering.

For group 9 the lower group boundary is located near a descending wing of a resonance (fig. 16). This gives rise to flux enhancement at the lower part of the group thereby increasing slowing-down collisions with respect to intragroup collisions, resulting in increasing values for $\langle\sigma_d\rangle$ with decreasing σ_o.

When one defines self-shielding factor f_d for slowing-down in accordance to [Ab64] as

$$\langle\sigma_d(\sigma_o)\rangle = f_d(\sigma_o) \cdot \langle\sigma_d(\infty)\rangle \qquad (4.23)$$

this factor will increase with decreasing σ_o if the lower boundary is positioned in a descending wing and it

will decrease if positioned in an ascending wing of a cross section resonance. In the ABN-set $f_d(\sigma_o)$ is a decreasing function with decreasing σ_o for all materials given in the set; according to the arguments given above this may give rise to considerable errors. Table III gives the results for the group from 21.5 keV to 46.5 keV.

	$<\sigma_d(\infty)>$	$f_d(\sigma_o=10)$	$f_d(\sigma_o=1)$	$f_d(\sigma_o=o)$
ABN	0.687	0.61	0.31	0.20
this work	0.0536	1.18	1.56	2.30

Table III. Self-shielding factors for the slowing-down cross section of aluminium in group 10 of the ABN-set (21.5 keV to 46.5 keV).

The discrepancy for $<\sigma_d(\infty)>$ is caused by the fact that $<\sigma_d>$ in the ABN-set is computed simply from $<\sigma_e>$ for elastic scattering which can be done only if the scattering cross section is energy independent within the group.

A second important effect is the influence of aluminium resonance scattering on the slowing-down cross section of graphite. Due to flux enhancement near the boundaries of groups 8, 9 and 10 the σ_d of graphite increases with increasing admixture of aluminium. For accurate calculation of the lower part of the flux spectrum the influence is important because in fast power reactors the spectrum shows a strong fine structure caused by the presence of structural materials such as iron, nickel and chromium. These materials do not give an important contribution to elastic slowing-down and therefore a re-evaluation of slowing-down cross sections for these materials may give only small modifications in spectra, but the effect of the strong flux variations on slowing-down cross sections of lighter elements such as beryllium, carbon and sodium may be rather strong as shown in Table II.

IV.4 Influence of neutron leakage on group cross section values; procurement of group cross sections from measured spectra

In the preceding paragraph an analysis has been presented of group cross section evaluation for infinite homogeneous systems. Neutron leakage in finite systems can be accounted for by adding a term to the LHS of Eq. (4.20):

$$\left\{ \Sigma_t(E) + \frac{B^2(E)}{3\Sigma_{tr}(E)} \right\} \phi(E) =$$

$$= \sum_i \int_E^{E/\alpha_i} \frac{\Sigma_{si}(E')\phi(E')}{E'(1-\alpha_i)} \, dE' + S(E) \quad . \qquad (4.24)$$

The source term of this equation is based on isotropic scattering in the C.M.-system for all nuclides (index i); the contribution of external sources is given by S(E). The term for net neutron leakage has been taken from diffusion theory (Eq. 3.14); the *flux buckling* has the conventional definition:

$$B^2 = - \nabla^2\phi \; / \; \phi \qquad (4.25)$$

The influence of neutron leakage on slowing-down cross sections can be understood easily. With increasing flux buckling (i.e. increasing neutron leakage), the ratio of the flux in the moderation region near the lower group boundary to the total group flux decreases, and as a consequence the slowing-down cross section decreases. The effect of leakage on the group cross sections for absorption, transport and intragroup scattering depends on the detailed cross section behaviour as a function of neutron energy. Eq. (4.24) can be applied in different ways. The first possibility is to use this equation to improve the accuracy of a multigroup transport calculation. In that case a multigroup space dependent calculation is performed with some standard cross section set; with the group bucklings then obtained, an improved cross section set is

evaluated using Eq. (4.24) and a second space dependent calculation can be started. After a few iterations a very accurate space dependent spectrum is obtained, provided the geometry of the system is treated properly and the energy dependent behaviour of the cross sections is well-known. The computational effort may be rather large, however, especially for non-multiplying systems where the neutron spectra can be strongly space dependent.

For the studies reported in this thesis another approach has been developed.

Here the *measured neutron spectra* are used to calculate group cross section values which are, within the framework of the multigroup treatment, consistent with the experimental data. For this purpose a computer code has been written which uses the measured spectra as input data and solves Eq. (4.24) for the group bucklings. In first approximation the flux buckling within each energy group is assumed to be energy independent and the detailed neutron spectrum is evaluated by solving the integral equation with an exact representation of the cross sections behaviour; with an iteration procedure the buckling values are calculated which are consistent with the measured group flux ratios. Further the detailed neutron spectrum is used to evaluate group cross sections with Eqs. (4.4) and (4.7).

Furthermore, the calculated neutron spectrum can be compared with the measured spectrum which may be useful because many details of the neutron spectrum are often lost in a multigroup calculation as a result of the rather large group widths. In this case it is necessary to account for detector resolution which can be done by convolution of the calculated detailed spectrum with the detector resolution function (*"smoothing with a gaussian window"*).

In the procedure described above the detailed neutron cross section behaviour is assumed to be well-known. The adequacy of this assumption in specific cases can be tested by analyzing the space dependence of the neutron spectrum and comparing the results with the buckling values obtained by solving Eq. (4.24). For critical assemblies, in which the flux buckling is not or only weakly energy- and space dependent, this method can be used in order to infer cross section information from experimentally determined neutron spectra.

V. RESULTS AND DISCUSSION

V.1 Introduction

In this Chapter the results of calculations and measurements on FANCY-cores will be presented and discussed. Fig. 17 shows a horizontal cross section through the centre of the FANCY-assembly; for position indication in the assembly a matrix numbering system is used.

The fission plates, mentioned before in II.1, were positioned in the elements indicated by the dashed area in fig. 17. In each element two plates were inserted in vertical position in such a way that the ^{235}U containing zone extended from 12.5 cm. below to 12.5 cm. above the horizontal core midplane; consequently the total ^{235}U content in the core amounted to 300 gm.

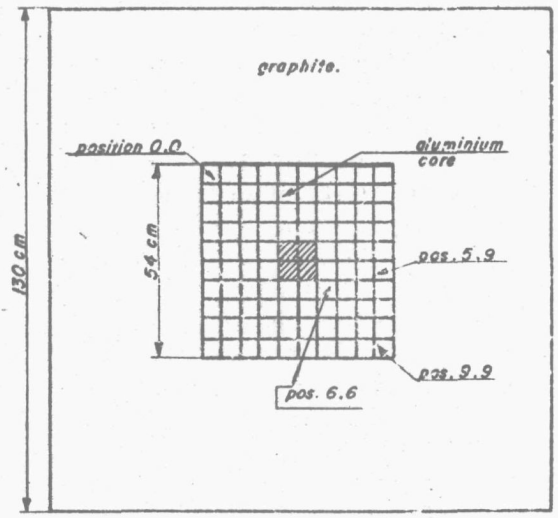

Fig. 17. Horizontal cross section through the centre of the FANCY-assembly.

For all measurements the detectors were positioned with the centre of the sensitive volume in the horizontal midplane through the centre of the FANCY-assembly. An axial cross section through a measuring element is shown in Fig. 18. For routine spectrum measurements the compositions of measuring element and core elements c.q. reflector elements were matched as closely as possible.

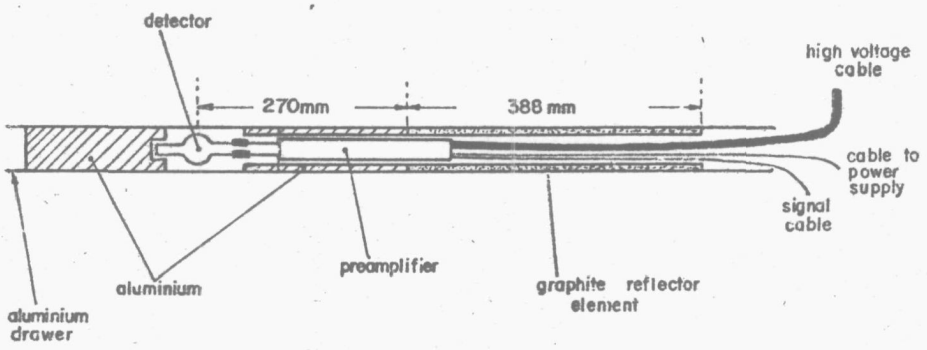

Fig. 18. Axial cross section through a measuring element.

In the lower part of the measuring element complete matching was possible, in the upper part half of the material had to be removed in order to create a circular channel for preamplifier and cables; for the determination of measuring channel perturbation all material in the upper part was removed. The detectors were surrounded by a 12x5x5 cm^3 cavity; for all the measurements reported here spherical detectors were used.

In this Chapter the various FANCY-cores are numbered I, II, and III. FANCY-I is a pure aluminium core, in which measurements of fast neutron spectra and the influence of measuring channels on these spectra have been performed. The assemblies FANCY-II resp. FANCY-III have been build up by inserting polyethylene resp. graphite containing elements in four symmetrical positions around the core centre.

V.2. Neutron spectra in FANCY-I

V.2.1. One-dimensional diffusion and S_n calculations

The results of one-dimensional S_4 calculations of the

space-dependent neutron spectrum in FANCY-I are shown in Fig. 19. For these calculations an one-dimensional model of the FANCY-assembly has been used, consisting of an aluminium sphere (radius = 33 cm) surrounded by a graphite spherical shell (thickness = 42 cm); this system is fed by a centrally positioned shell shaped fission source extending from r = 5 cm to r = 6 cm.

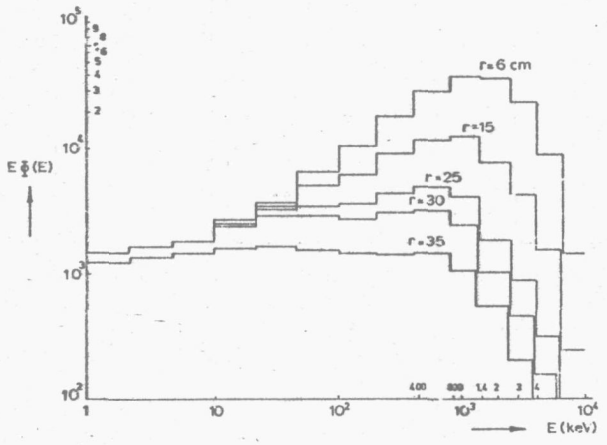

Fig. 19. Neutron spectra in FANCY-I, calculated with a one-dimensional model.

Use has been made of the ABN cross section set [Ab64] with the aluminium cross sections of groups 7 to 11 modified according to Table II of Chapter IV with self-shielding factors for pure aluminium. Due to fabrication tolerances the core contains 7 v/o air, which is considered as being equivalent to vacuum (the mean free path of fast neutrons in air is about 50 m) and distributed homogeneously in the core.

In Table I the group structure of the ABN-set for the energy interval from 1 keV to 10.5 MeV is presented.

It can be seen in Fig. 19 that radially outward from the core centre the spectrum softens continuously and approaches a 1/E-distribution (constant flux per unit of lethargy interval) in the reflector. In the low energy tail of the spectrum the flux level is almost spatially independent in the aluminium zone due to a large supply of moderated neutrons coming from the graphite, and because of the large diffusion length of these neutrons

in aluminium (the mean free path of neutrons with an energy of about 25 keV, which give a large contribution to the neutron flux in group 10, amounts to 35 cm).

group:	lower boundary:	group:	lower boundary:
	10.5 MeV		
1	6.5	8	100 keV
2	4.0	9	46.5
3	2.5	10	21.5
4	1.4	11	10
5	800 keV	12	4.65
6	400	13	2.15
7	200	14	1

Table I. Group structure of ABN-set [Ab64].

A comparison between the results of S_4 and diffusion calculations is shown in Fig. 20. In accordance with the

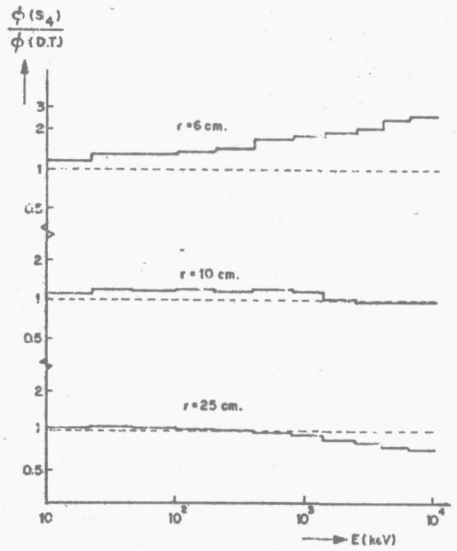

Fig. 20.
Comparison between the results of S_4 and diffusion calculations for FANCY-I.

considerations given in paragraph III.4, the diffusion calculation shows an underestimation of flux levels in positions near the source, in particular at higher energies. Therefore spectra obtained at these positions as a result of diffusion calculations are too soft; at positions farther than a few mean free paths from the source the diffusion spectra are too hard.

V.2.2. Influence of anisotropic scattering

In order to assess the influence of scattering anisotropy on the neutron energy distributions in FANCY-I, a study has been made with the anisotropic scattering version of the code FAST-DSN-DELFT [Br69]. Flux anisotropy was handled in S_4 approximation. Data concerning the angular distribution of scattering by aluminium and graphite were taken from Ref. [Ca67].

In Fig. 21 a comparison is given between five approximations which in order of increasing accuracy can be listed as:

a. P_0 approximation: all scattering is assumed to be isotropic
b. diagonal transport approximation
c. corrected diagonal transport approximation
d. P_1 approximation: the angular distribution of scattering is treated exact up to the second Legendre component.
e. P_2 approximation: just like method d but up to the third Legendre component.

It has been shown in the paragraphs III.2 and III.3 that the transport approximations give good results provided scattering is either isotropic or can be considered as consisting of an isotropic component plus a purely forwardly directed component. This explains the large discrepancies in the intermediate energy region (0.1 MeV - 1 MeV) where neither of these conditions is fulfilled. At larger distances from the source, however, the transport approximations give satisfactory results. The P_1 solution is more acuurate but for most cases the transport approximation is preferable because of the less computational effort required. It may be noted that, in accordance with the analysis presented in Chapter III, the DTA scheme can be more accurate than the CDTA scheme in the high energy part of the spectrum; in this part the

flux is rapidly decreasing with increasing energy which implies that anisotropic down scattering from each energygroup is not compensated for by anisotropic moderation from higher energy groups.

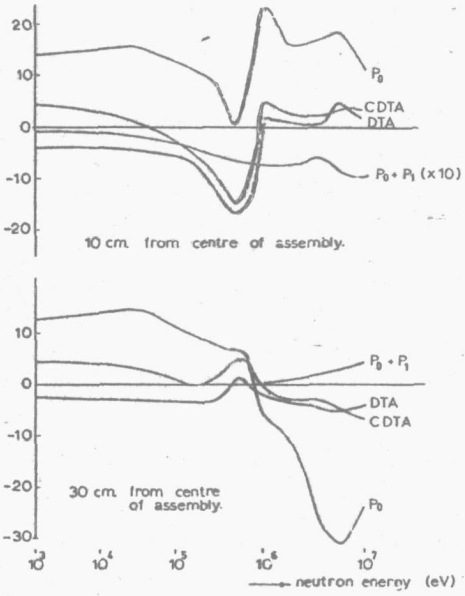

Fig. 21.
Discrepancy (%) of the group flux levels as introduced by approximations indicated and calculations, incorporating scattering anisotropy up to P_3 components (one-dimensional model of FANCY -I).

V.2.3. Two-dimensional S_n calculations

For the two-dimensional S_n calculations, the FANCY-core is assumed to have infinite dimensions in the axial direction of the elements. For the FANCY-I core this approximation is inadequate; in fact this type of calculations, performed with the code XYSNI [Ho70], is useful only to *assess* flux perturbations caused by local heterogeneities such as measuring channels and moderating or absorbing materials.

The spectra at three positions in FANCY-I, calculated with the code XYSNI, are shown in Fig. 22. These spectra are, especially near the fission plates, significantly softer than those calculated for the one-dimensional model, which is caused by the much lower neutron leakage in the two-dimensional model (which means a larger probability

for neutrons to be moderated without leaking out of the system).

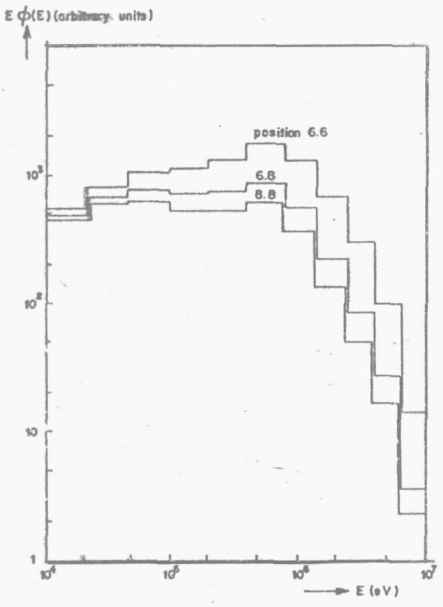

Fig. 22.
Results of two-dimensional calculations on FANCY-I.

During the development of the code XYSNI, some difficulties have been encountered which could be identified as being caused by the so-called "ray-effect". This effect, first published by Lathrop [La68], is characteristic for more-dimensional S_n calculations on non-multiplying systems with a small external source. An illustration for a fictitious system is given in Fig. 23. In case the angular discretization is too coarse, some areas in the system do not "see" the neutron source, in particular when absorption is strong in comparison with scattering. For demonstration purposes, the case of a purely absorbing medium has been chosen in Fig. 23, with the additional advantage that an analytical solution of the transport problem is straightforward.

A trivial method to avoid ray-effects is to increase the order of the angular quadrature [La68]. For this reason the code XYSNI has the special feature of *group-dependent order of angular quadrature*. In the highest

energy groups, where the slowing-down scattering is large compared to intragroup scattering, it often appears to be necessary to refine the angular discretization. For the calculations on FANCY-I it was necessary to use S_{12} approximations in the three energy groups above 2.5 MeV, S_8 in the five groups between 100 keV and 2.5 MeV and S_6 for the lower energy groups. The number of discrete directions in two-dimensional S_n calculations amounts to $n(1 + 0.5\ n)$, which implies that for the cases studied here rather time-consuming calculations were necessary for the high energy groups.

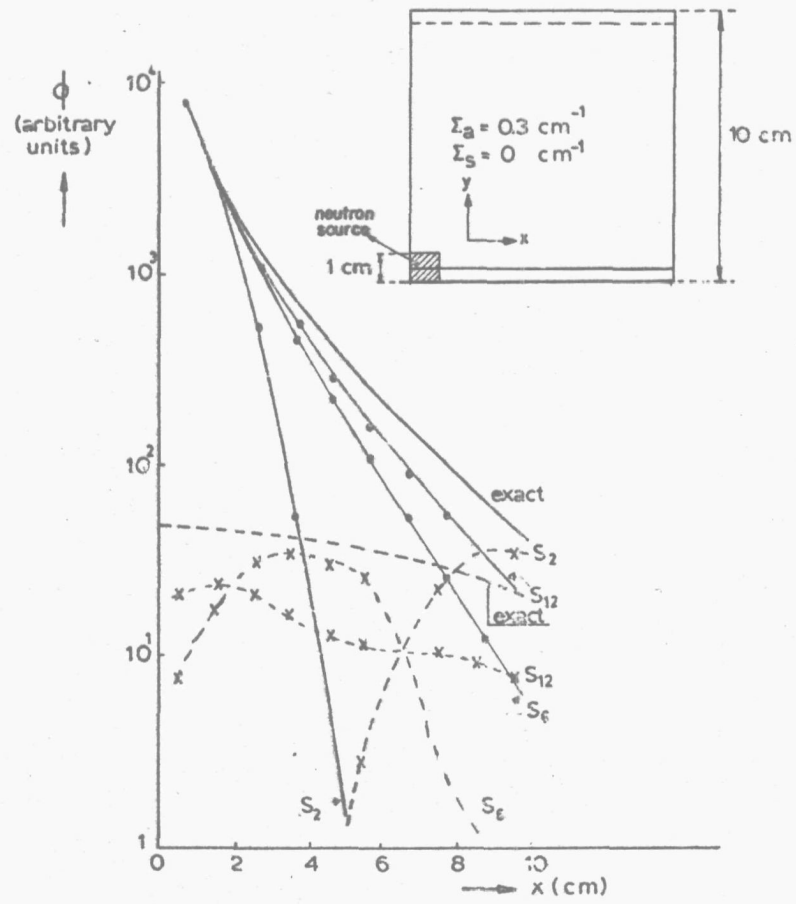

Fig. 23a. Ray-effect in two-dimensional S_n calculations; the solid resp. dotted lines in the graph refer to the flux distributions along the solid resp. dotted line shown in the sketch of the system geometry.

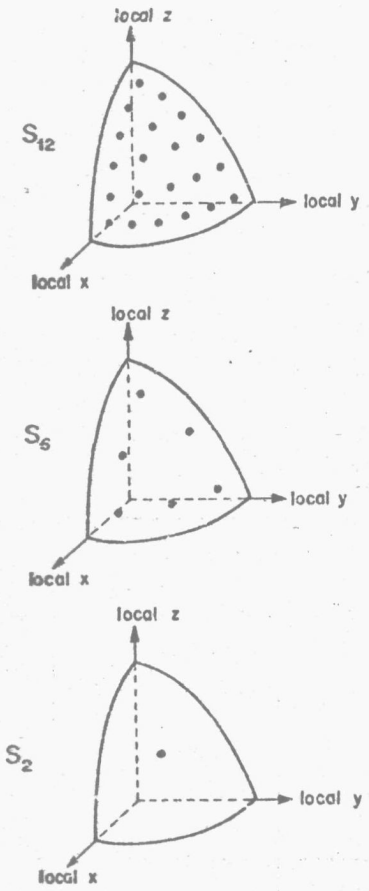

Fig. 23b.
Angular discretization for different S_n approximations; each direction in one quadrant of the upper hemisphere is represented by a point.

Therefore another approach has been developed, based on *group collapsing* of the three highest energy groups. Group-cross sections for the so-obtained group, extending from 2.5 MeV to 10.5 MeV were calculated with formulas, consistent with Eqs. (4.4) to (4.7) i.e.:

$$\langle \sigma_{tr} \rangle = \sum_{i=1}^{3} \phi_i \Big/ \sum_{i=1}^{3} \phi_i \, \sigma_{tr,i}^{-1} \tag{5.1}$$

$$\langle \sigma_c \rangle = \sum_{i=1}^{3} \sigma_{ci} \, \phi_i \Big/ \sum_{i=1}^{3} \phi_i \tag{5.2}$$

$$< \sigma_d > = \sum_{i=1}^{3} \sum_{k>3} \sigma_{ik} \phi_i \Big/ \sum_{i=1}^{3} \phi_i \qquad (5.3)$$

The fission neutron spectrum was taken as averaging spectrum; for physical reasons this averaging spectrum is adequate for positions not too far from the fission plates. From Table II is concluded that this method yields fairly accurate results.

The savings in computer time are considerable for two reasons:

1. three energy groups are collapsed into one group
2. due to the lower removal-to-intragroup scattering ratio the influence of ray-effects is diminished (compare S_{12} vs. S_8 results in Table II), which allows a low order of angular quadrature.

angular quadrature	energy range	position 6.6	position 8.8
S_{12}	2.5 MeV-10.5 MeV	+1.7%	+5.2%
	1.4 MeV- 2.5 MeV	-0.9%	-0.8%
	0.4 MeV- 1.4 MeV	-0.4%	-0.2%
	below 0.4 MeV	less than 0.1%	less than 0.1%
S_8	2.5 MeV-10.5 MeV	+2.6%	+5.5%
	1.4 MeV- 2.5 MeV	-0.8%	-0.8%
	0.4 MeV- 1.4 MeV	-0.4%	-0.2%
	below 0.4 MeV	less than 0.1%	less than 0.1%

Table II. Effect of group collapsing in two-dimensional S_n calculations; indicated by the relative differences between flux values obtained as a result of calculations with resp. without collapsing of the groups between 2.5 MeV and 10.5 MeV.

In the calculation of reactor cores ray-effects may occur near local heterogeneities, such as control rods

which act as negative sources with rather small dimensions. In a recent study [Mi70] it is shown that overlooking of ray-effects can lead to erroneous conclusions in fast reactor core design studies.

V.2.4. *Coarse and fine group calculations; space dependence of group cross sections in FANCY-I*

When a system consists of a heterogeneous composition of a resonance scatterer and a potential scatterer it is possible to evaluate appropriate group cross sections by using cross section tables for homogeneous mixtures, e.g. as given in IV.3; in that case one has to calculate an effective σ_o for the resonance scattering material by means of an equivalence theorem [Dr60]. This method is feasible only if the mean chord lengths (i.e. the mean distances travelled in the zones by neutrons in case of zero cross section) of the zones containing the resonance scattering components are small compared to the mean free path of neutrons in this material. The system studied here, however, consists (in one-dimensional approximation) of an aluminium sphere (radius = 33 cm) surrounded by a graphite spherical shell (thickness = 42 cm). This system is fed by a centrally positioned shell shaped fission source extending from r = 5 to r = 6 cm.

Calculation results with the ABN-set showed strongly space-dependent spectra (Fig. 19) and as a consequence the group cross sections, especially those for groups containing scattering resonances, will be space-dependent.

In order to assess this space dependence and the discrepancies in calculated flux levels caused by neglecting this effect two calculations were performed:

1. a calculation with group cross sections for pure aluminium (i.e. σ_o = o) in the core and for graphite in the reflector. The group structure of the ABN-set has been adopted, cross sections were adjusted according to Table II, method C of Chapter IV.
2. a calculation with the four energy groups between 21.5 keV and 400 keV each divided into 5 subgroups with equal lethargy-width. Group cross sections for these subgroups were calculated according to method C outlined in IV.3.

From the second calculation space-dependent group cross sections for the broad groups of the ABN-set can be deduced. Some results are given in Table III and Figs. 24 en 25.

r(cm.):	group 10 (21.5 keV-46.5 keV) σ_t:	σ_d:	$(\phi_2-\phi_1)/\phi_1$(%):	group 9 (46.5 keV-100 keV) σ_t:	σ_d:	$(\phi_2-\phi_1)/\phi_1$(%):
0	0.863	0.0470	1.5	1.99	0.133	-1.1
5	0.885	0.0460	2.0	2.03	0.133	-0.8
10	0.827	0.0514	0.1	1.94	0.146	+1.6
14	0.813	0.0534	-0.1	1.92	0.154	3.4
20	0.801	0.0559	-0.6	1.90	0.164	5.0
24	0.797	0.0573	-1.1	1.89	0.172	5.0
30	0.815	0.0584	-1.6	1.90	0.187	4.2
33	0.884	0.0569	-1.2	2.01	0.199	6.7
cross sections used for broad group calculations	0.611	0.122		1.82	0.228	

r(cm.):	group 8 (100 keV-200 keV) σ_t:	σ_d:	ϕ_2/ϕ_1:	group 7 (200 keV-400 keV) σ_t:	σ_d:	ϕ_2/ϕ_1:
10	2.75	0.268	1.064	3.23	0.307	1.163
20	2.69	0.304	1.085	3.23	0.350	1.121
30	2.67	0.319	1.058	3.23	0.371	1.063
cross sections used for broad group calculations	2.64	0.346		3.24	0.358	

Table III. Space dependence of group cross sections in FANCY.

ϕ_1: group flux calculated with ABN [Ab64] group structure

ϕ_2: group flux calculated with fine group structure.

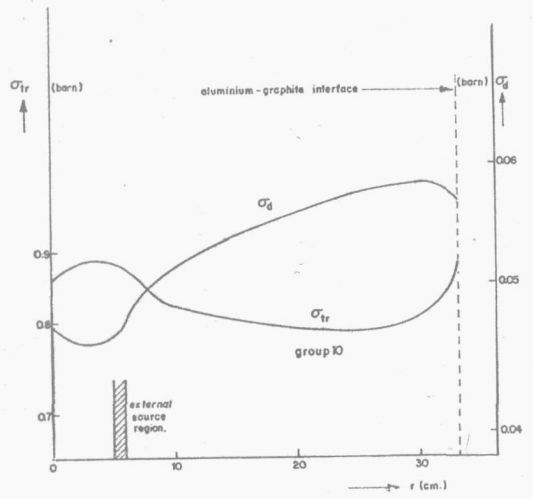

Fig. 24.
Space dependence of transport and slowing-down cross sections (group 21.5 keV-46.5 keV) in FANCY-I.

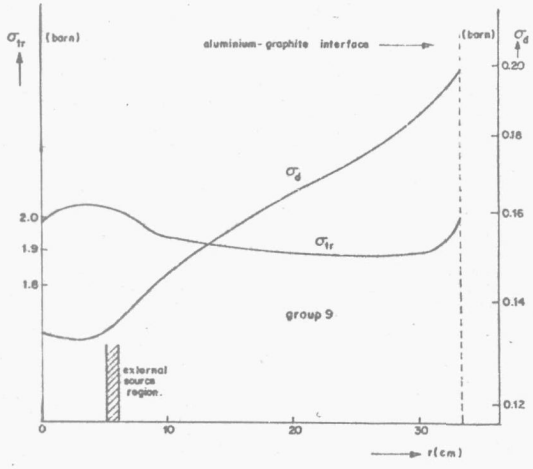

Fig. 25.
Space dependence of transport and slowing-down cross sections (group 46.5 keV-100 keV) in FANCY-I.

The space dependence of the group cross sections, in particular the slowing-down cross sections, is rather strong. For a qualitative explanation of the space dependence, it has to be considered that resonance self-shielding at positions near the source and in the vicinity of the core-reflector interface is less than in other positions. The reason why, is, that near the source the flux dips in the spectrum are partially filled up by both first-flight source neutrons and neutrons which have suffered only a few collisions. Near the reflector,

smoothing of flux dips is caused by neutrons diffusing from the graphite into the aluminium core.

The sensitivity of the group fluxes to cross section variations appears to be rather limited which is due to partical cancellation of errors. An underestimation of the total cross section gives an underestimation of flux levels due to overrated neutron leakage; if the slowing-down cross section is too low, the flux in the group considered is too high as a consequence of underestimation of neutron removal by slowing down. Moreover, these effects extend to all lower energy groups; e.g. in the particular case considered here, the very small flux deviations in group 10, in despite of rather large errors in the group cross sections are the result of compensating effects in group 9.

V. 2.5. Experimental aspects

For the spectral measurements reported in this thesis, spherical proportional counters (fig. 6) have been used with two different gasfillings:
5 bar CH_4 for the energy region from 0.4 MeV to 3 MeV
4 bar H_2 for the energy region below 1 MeV

At the upper energy limits about 80% of the recoil protons collide with the detector wall; the neutron spectra above resp. 2.5 MeV and 0.8 MeV obtained from the measured recoil proton spectra were disregarded in order to reduce errors caused by the "fast neutron effect" (Fig.8).

All measurements were normalized on the basis of counting results of a monitor channel with a BF_3 detector, located at the outer boundary of the graphite reflector of FANCY, to the same fluence of neutrons from the thermal column.

For energies under 150 keV it was necessary to apply the gamma discrimination technique, described in Chapter II. Gamma discrimination has been applied only to the hydrogen detector measurements because of the low electron drift velocity under the influence of an electric field in this gas compared to methane [Ma60]; therefore the lower energy limit for the methane detector is determined by the gamma response.

In FANCY the gamma-to-neutron ratio is very high in comparison to the γ/n-ratio in actual reactor cores, (Table IV). This is due to the high thermal flux in

FANCY compared to the fast neutron flux, which leads to a high production of capture and activation gamma rays; moreover, aluminium has rather inferior gamma shielding properties. Hence, the lower energy limit for the spectrum measurements (which is determined by the gamma-to-neutron ratio) was approximately 20 keV. Because the use of the cylindrical detectors implies an increase in the gamma level (Chapter II.2.3), it was decided to perform all measurements in FANCY with spherical detectors.

System:	$\gamma/n[rem.hr^{-1}/n.cm.^{-2}s^{-1}]$(neutron energy above 10 keV)
FANCY	2.10^{-4}
Secondary Standard Facility at Mol [Fa68,Le70]	6.10^{-7}
Heavy Water Reactor [Be64]	8.10^{-7}
Materials Testing Reactor [Be64]	7.10^{-7}
Fast Breeder Reactor	2.10^{-7}

Table IV. Gamma-to-neutron ratios in different facilities.

The drawbacks of a high γ/n-ratio are both the limitation of the energy-range that can be covered by the measurements, and the long measuring times needed to obtain sufficient statistical accuracy. For each run about 5.10^7 proton counts must be accumulated; because the count-rate is limited to about 3000 s^{-1}, as a consequence of detector and electronic equipment properties, this implies a measuring time of 5 hours for each run in case of no gamma response. In principle the measuring time is proportional to the ratio of total counts to proton counts. Because the measurement of a single neutron spectrum in the range from 20 keV to 2.5 MeV involves three separate runs, of which one has to be performed with gamma discrimination, a measuring time of a few days is required for sufficient statistical accuracy. Data were accumulated in a multi-channel analyzer, punched on paper tape and further processed in the IBM 360/65 computer of the Delft University of Technology.

V. 2.6. Results of measurements in FANCY-I

Results of measurements and of two-dimensional S_n-calculations for the positions 6.6, 6.8 and 8.8 in FANCY-I are presented in Figs. 26,27 and 28. The statistical accuracy of the group fluxes is better than 1%. In the same figures the background spectra, measured after removal of the fission plates, are shown; these spectra are very soft due to the many moderating collisions suffered by reactor neutrons before entering into the FANCY-core.

In Table V the results of measurements (background fluxes subtracted) and of one- resp. two-dimensional S_n-calculations are presented, normalized on the flux of group 6 in position 6.6 (rather arbitrarily chosen); the radial coordinates in the one-dimensional spherical model are selected equal to the distances between the core centre and the detector centre in the three positions.

The total flux deviation indicates the differences between measured and calculated values for the total flux between 21.5 keV and 2500 keV, resp. 21.5 keV and 800 keV. It can be concluded that the one-dimensional model better predicts the space-dependence of the flux, especially in the region under 800 keV. The spectra under 800 keV predicted by two-dimensional S_n-calculations are too soft, which has already been explained qualitatively in V.2.3. It is remarkable that the flux gradient of the highest energy flux is in rather good agreement with the two-dimensional calculation. This can be partially explained by the influence of scattering anisotropy which tends to flatten the radial dependence of the high-energy flux (Fig. 21).

In Figs. 29,30 and 31 the detailed spectra in the energy region from 25 keV to 500 keV are presented; the standard deviation of the flux values is approximately inversely proportional to the flux values and is indicated for some measuring points, the relative energy resolution amounts to about 15%. The solid curves drawn in these figures are obtained by solving Eq.(4.24) with a computer code mentioned in IV.4, taking account of the detector resolution. From the comparison of measuring points and the theoretical curves it is evident that the structure in the measured spectrum is less pronounced than in the theoretical one. This is

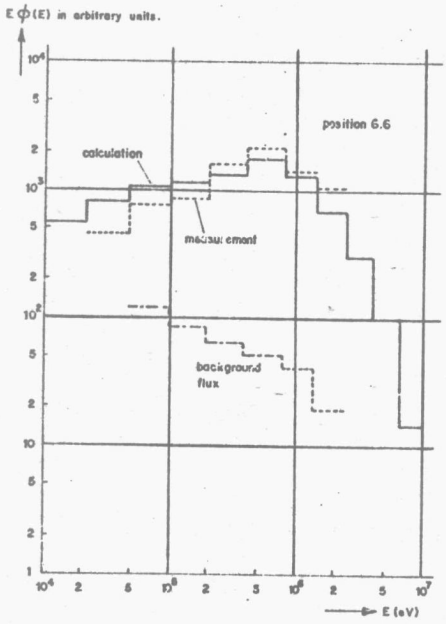

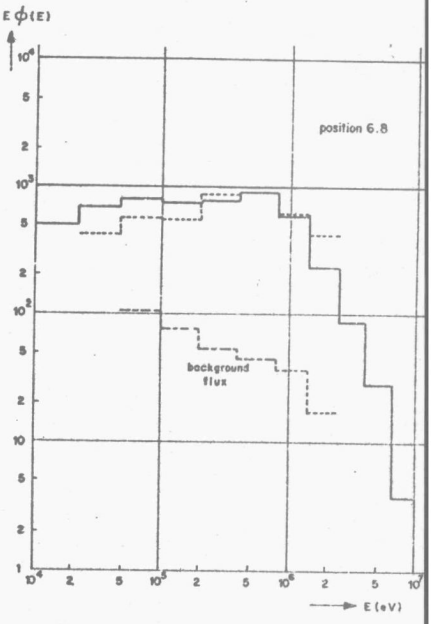

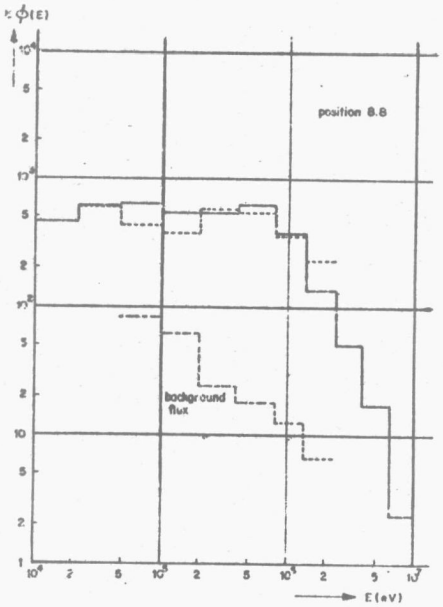

Figs. 26,27,28.
Measured and calculated (two-dimensional model) spectra in positions 6.6, 6.8 and 8.8 of FANCY-I.

position:	group:	ϕ (measured):	ϕ (one-dim. calculation):	ϕ (two-dim. calculation):
6.6	4	0.53	0.69	0.41
	5	0.74	1.05	0.77
	6	1.00	1.00	1.00
	7	0.76	0.72	0.79
	8	0.43	0.45	0.67
	9	0.34	0.33	0.62
	10	0.15	0.24	0.48
total flux deviation		(groups 4-10)	+ 13%	+ 20%
idem		(groups 6-10)	+ 2%	+ 13%
6.8	4	0.20	0.15	0.14
	5	0.29	0.32	0.35
	6	0.45	0.38	0.54
	7	0.41	0.33	0.47
	8	0.24	0.24	0.44
	9	0.24	0.22	0.48
	10	0.14	0.17	0.41
total flux deviation		(4-10)	- 8%	+ 44%
idem		(6-10)	- 9%	+ 58%
8.8	4	0.12	0.068	0.080
	5	0.18	0.16	0.22
	6	0.27	0.23	0.36
	7	0.28	0.22	0.32
	8	0.14	0.17	0.32
	9	0.16	0.17	0.37
	10	0.21	0.15	0.36
total flux deviation		(4-10)	- 14%	+ 50%
idem		(6-10)	- 11%	+ 63%

Table V. Results of measurements and one- resp. two-dimensional S_n-calculations in FANCY-I.

$$\text{Total flux deviation} = \sum_g \frac{\phi_g(\text{calculated}) - \phi_g(\text{measured})}{\phi_g(\text{measured})} \cdot 100\%$$

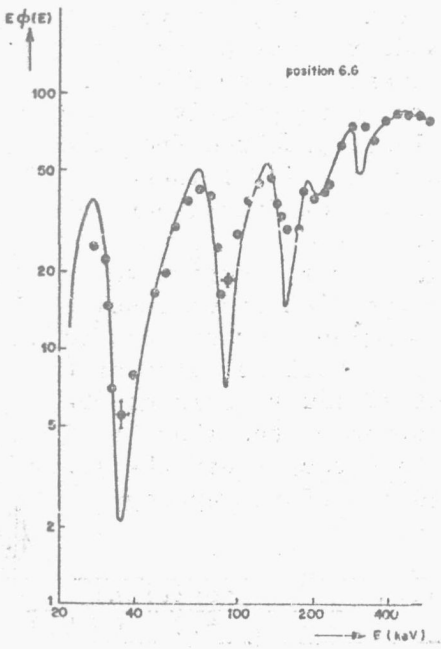

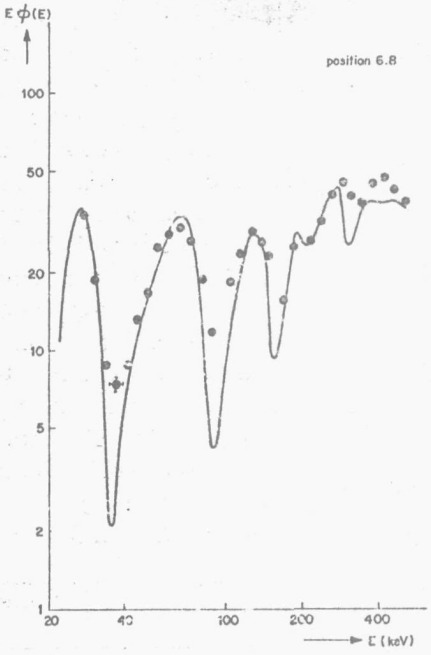

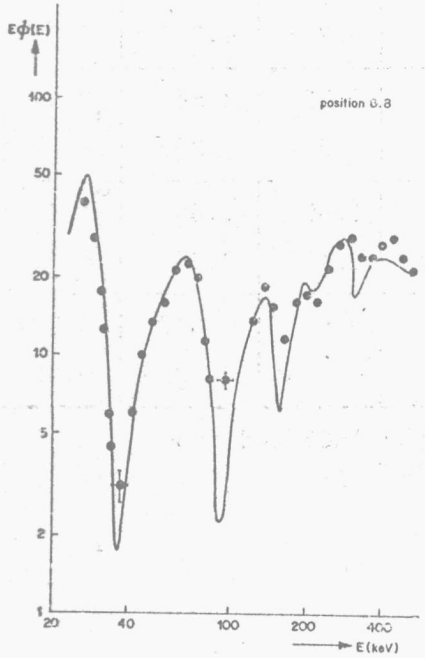

Figs. 29,30,31.
Measured and calculated detailed neutron spectra in FANCY-I, positions 6.6, 6.8 and 8.8.

caused by the fact that the contribution of first-flight source neutrons (which have a smooth energy distribution) is neglected in the calculation of the theoretical spectra. The spectra calculated with the fine group structure described in section V.2.4. show peak-to-valley flux ratios which are more consistent with the experimental results; the relative group width ($\Delta E/E$) in the fine group set is about 15%, which is equal to the detector resolution. It should be kept in mind, however, that the smoothing of the measured spectrum may be partially caused by some gamma interference in the flux minima, where the gamma-to-neutron ratio is relatively high.

Group cross section values, procured from the detailed spectra, are given in Table VI. These values can be compared with the results of fine group calculations presented in Table IV.

For group 7 the transport cross section values are in very good agreement with the fine group results. The space-dependence of the slowing-down cross section shows a good consistency but for the absolute value of the cross section which is about 7% lower; this can be explained by the underestimation of the flux level in the moderation-interval of the group (near the lower group boundary) as a consequence of the energy-independent buckling concept.

group:	cross section:	position:		
		6.6	6.8	8.8
7	σ_{tr}	3.26	3.24	3.23
200-400 keV	σ_d	0.283	0.327	0.358
8	σ_{tr}	2.79	2.86	2.96
100-200 keV	σ_d	0.291	0.259	0.231
9	σ_{tr}	1.90	1.83	1.83
46.5-100 keV	σ_d	0.143	0.200	0.250
10	σ_{tr}	0.68	0.877	0.704
21.5-45.5 keV	σ_d	0.0285	0.0275	0.063

Table VI. Group cross sections inferred from measurements in FANCY-I.

For group 8 the results for the slowing-down cross section are in conflict with the results of the fine group calculation. In particular a discrepancy in space-dependence is evident. An explanation of this discrepancy may be found in the fact that in the fine-group calculation the width of the groups is sufficiently small compared to the width of the aluminium scattering resonances, except for the group from 115keV-132 keV, for which the boundaries are positioned in the cross section minima of a sharp resonance at 120 keV.

For group 9 the results are rather consistent with the results of the fine group calculations; the space-dependence of the slowing-down cross section, derived from the measurements, is more pronounced. The data given for group 10 can not be considered as reliable, because in the energy region near the lower boundary of this group the spectral information is inaccurate as a consequence of the high gamma level in FANCY.

The inaccuracy of the measured group fluxes is estimated at 5%, about 1% inaccuracy is due to counting statistics, the remaining 4% is due to fast neutron effect (Fig.8), inaccuracy in detector gas pressure (which influences the efficiency, wall-effect corrections and calibration) and electronic drift phenomena in both spectrometer and monitor equipment. Further errors are introduced by the energy resolution of the detector in case of strong flux variations near group boundaries.

The consequences of possible group flux inaccuracies for the group cross sections, as given in Table VI, can be illustrated by assuming an error of + 5% in the group flux. This leads to following cross section deviations at position 6.6:

	transport cross section:	slowing-down cross section:
group 7	- 0.2%	+ 4%
group 8	- 0.8%	+ 4%
group 9	- 0.8%	+ 5%
group 10	- 2.5%	+ 10%

It should be noted that these values only give an indication of the influence of a group flux error on the cross sections of the same group; actually, such an error also influences the results for lower energy groups, albeit to a less extent.

V.3. *Flux perturbations caused by detector channels*

Flux perturbation caused by a detector channel has been studied by applying two-dimensional S_n-analysis on FANCY-I. In these calculations the assembly is considered to be infinitely long in the direction of the detector channel.

Figs. 32 and 33 show the calculated flux perturbations caused by detector channels respectively in position 6.6 and 5.10. In the same graphs the local net

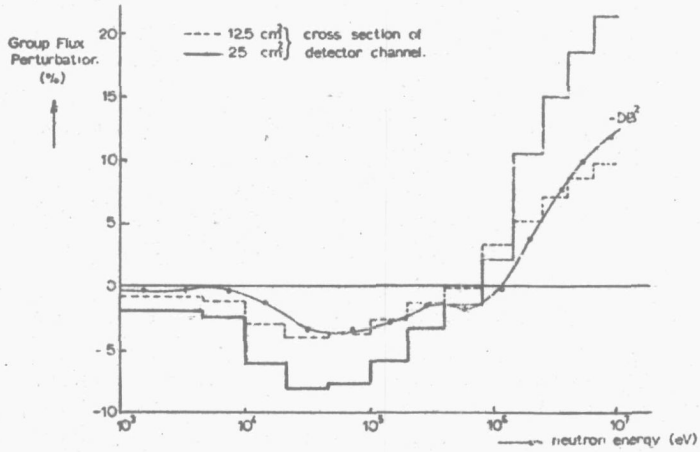

Fig. 32. Calculated flux perturbations caused by a detector channel in FANCY-I position 6.6 (two-dimensional model).

neutron in-flow per unit volume in the unperturbed system as a function of neutron energy has been given. These curves are indicated by the diffusion theory term $-DB^2$, i.e. diffusion coefficient multiplied by a negative buckling. From these curves the qualitative conclusion can be drawn that, when the local net neutron leakage per unit volume in the unperturbed system is negative- which means that the neutron absorption in the group considered exceeds the neutron production-, the introduction of a detector channel (removal of material) will lead to flux enhancement and vice versa, which is plausible from physical point of view. In this context neutron production includes moderation from higher energy groups; slowing-down to lower energy groups is

from a neutron balance point of view equivalent to absorption. It is interesting to note the remarkable difference in perturbation in the intermediate energy range at the positions 6.6 (near the fission source) and 5.10 (in the graphite reflector near the core reflector interface). It may be expected that flux levels in all energy groups will be lower than indicated by these calculations because of axial neutron streaming in the detector channel in the actual situation.

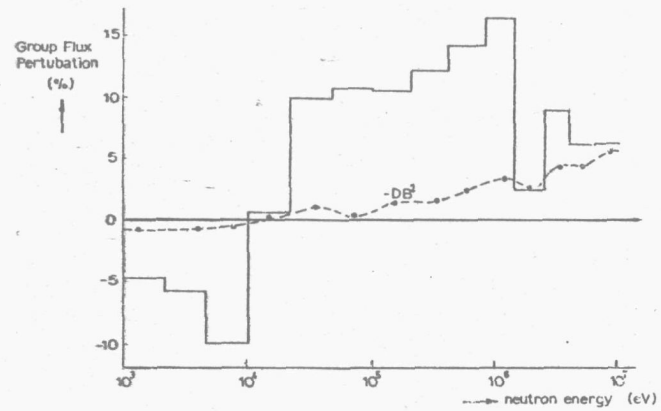

Fig. 33. Calculated flux perturbations caused by a detector channel in FANCY-I position 5.10 (two-dimensional model).

Measurements of flux perturbation by a detector channel have been performed by measuring spectra in positions 6.6 and 5.10 respectively with a normal detector element and an element, in which all material (aluminium + graphite) in the upper part had been removed. Results are shown in Figs. 34 and 35. The considerable discrepancies between experimental and theoretical values indicate that axial streaming of neutrons in the detector channel plays a predominant role, which is due to the fact that this channel passes through a region with a rapidly changing integrated flux and spectrum [Ca68]. The spectral hardening, caused by a detector channel inside the aluminium core, is rather well predicted by theory, but the flux level is over-predicted by about 10%. In position 5.10 the flux

discrepancy amounts to 10%-20% and a shift in horizontal direction between the two curves is observed. Because, in this position, the energy distribution of the neutrons in the high energy region is a complex result of elastic

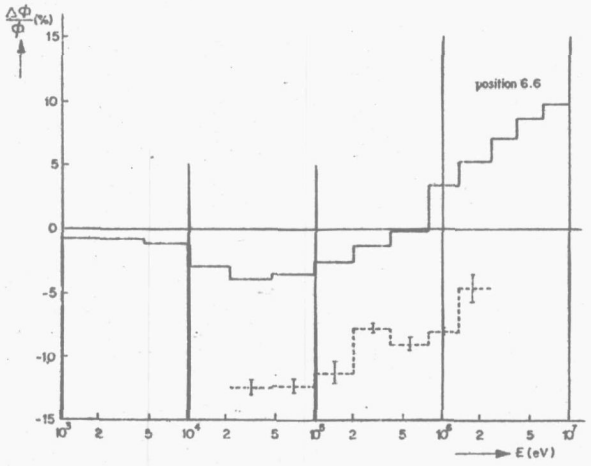

Fig. 34. Measured and calculated flux perturbations caused by a detector channel in FANCY-I position 6.6.

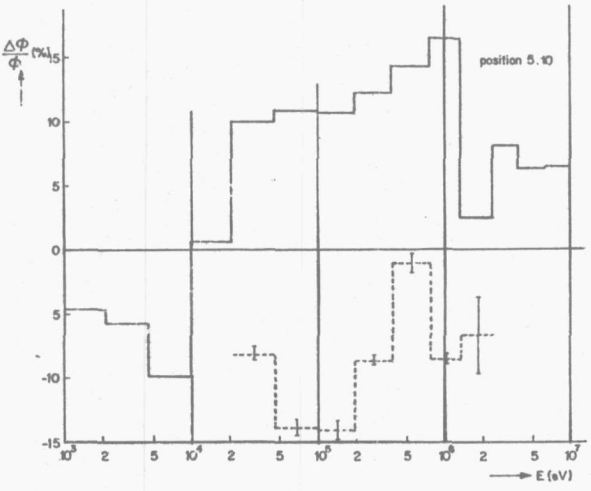

Fig. 35. Measured and calculated flux perturbations caused by a detector channel in FANCY-I position 5.10.

and inelastic moderation processes in two different materials, a qualitive explanation cannot be given for this discrepancy. For a better prediction of flux level shifts it is necessary to perform calculations in which the geometrical properties of the system are treated more accurately.

V.4. Results of measurements in FANCY-II and FANCY-III; flux perturbations caused by moderating materials.

Measurements and calculations have been performed to determine the influence of moderating materials, i.e. polyethylene and graphite, on the energy-dependent neutron flux in the FANCY-core. For the measurements four elements with moderating materials were positioned in symmetrical positions around the core centre, i.e. in the positions 2.2, 2.7, 7.2 and 7.7 (see Fig.17); this symmetrical positioning was used in order to save computer time and memory space for the two-dimensional S_n-calculations.

The graphite elements were completely filled with graphite, the polyethylene elements contained 50 volume percent (v/o) of polyethylene in the form of a centrally located polyethylene rod with 40 mm diameter; for the calculations the polyethylene containing elements were assumed to consist of a homogeneous mixture of 50 v/o polyethylene and 50 v/o aluminium.

With a BF_3-detector, positioned near the fission plates, it was ascertained that the insertion of the moderator elements did not affect the neutron density in the fission plates by more than 0.5%. Hence, the calculations of the spectral perturbations could be based on the assumption of a constant fission source strength.

The results obtained with polyethylene elements are shown in Figs. 36, 37 and 38. Both the measurements and calculations indicate a spectral hardening in the energy region above 20 keV and a spectral softening below this energy. This can be understood from the fact, that on the average the energy of the neutrons decreases strongly when colliding with the hydrogen nuclei of the polyethylene. Therefore, polyethylene acts as an "absorber" for high-energy neutrons and as a "source" for low-energy neutrons; according to S_n -

calculations, the cross-over point between flux decrease and flux increase is between 100 eV and 1 keV. The mean free path of neutrons in polyethylene decreases from 0.7 cm at 10 keV to about 10 cm. at 10 MeV, which explains the decreasing perturbation with increasing neutron energy: for high-energy neutrons the polyethylene rod is rather "transparent".

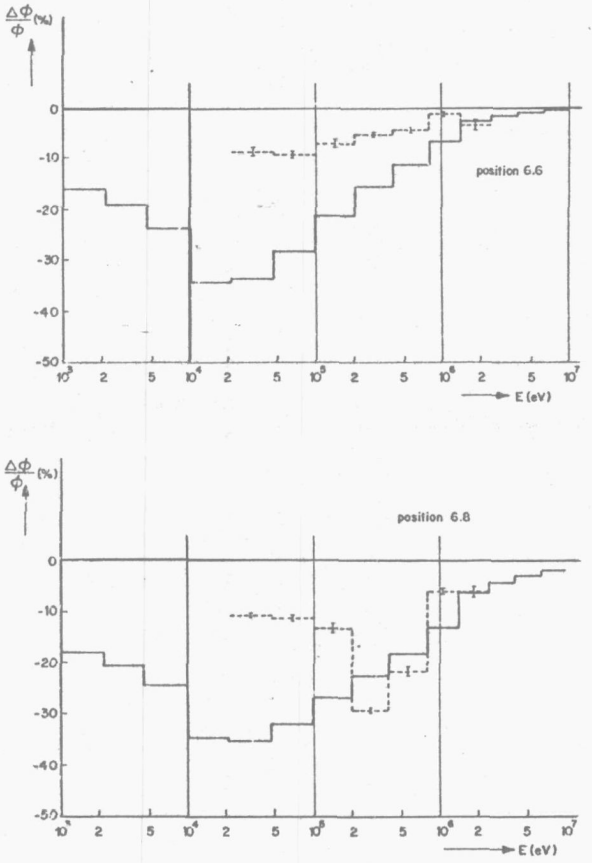

Figs. 36 and 37. Calculated (solid line) and measured relative flux perturbations caused by the insertion of polyethylene rods in FANCY-I, positions 6.6 and 6.8.

The measured perturbations are considerably smaller than those calculated, which is partly due to the limitations of the two-dimensional model used for the

calculations. In this model the moderator rods are assumed to be infinitely long, which leads to an overestimation of flux perturbation. It has to be considered that the harder the unperturbed spectrum, the less negative the flux perturbation, because for each energy group the source term due to moderation is enhanced relative to the absorption; in the fictitious case of a monoenergetic neutron field, the introduction of polyethylene leads to flux increase in the lower energy part of the spectrum. Because the unperturbed spectrum in FANCY-I is calculated too soft, it is evident that the flux perturbation at intermediate energies is overestimated. It must be noted here that the error margins indicated in Figs. 36, 37 and 38 only refer to uncertainties arising from counting statistics; evidently the measurements results between 200 keV and 800 keV in assembly position 6.8 are unreliable due to an unknown experimental error.

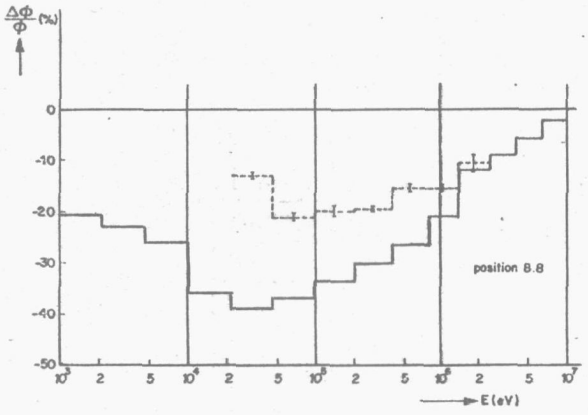

Fig. 38. Calculated and measured relative flux perturbations caused by the insertion of polyethylene rods in FANCY-I, position 8.8.

Studies have been made of the influence of the type of transport approximation used for the treatment of anisotropic scattering. For the calculated results shown, the CDTA-scheme was used. Use of either the DTA-scheme or completely neglecting scattering anisotropy

leads to differences in calculation results which are small compared to the discrepancies observed between theory and experiment.

An effect which has not been taken into account for the calculation results shown in Figures 36 through 38, is the influence of the polyethylene rod on the effective group cross sections of the aluminium surrounding the rod. In Table VII data are presented of the flux behaviour in the energy region of the 35 keV and 88 keV resonances of aluminium, both with and without polyethylene rod inserted; at the energies selected there is either a flux maximum or flux minimum (see Figs. 29, 30, 31). Additionally, values are given for the total mean free path of neutrons (M.F.P.) in aluminium at the particular energies.

Neutron energy (keV):	35	65	88	110	130
M.F.P. (cm):	0.5	12.5	1.0	9.0	1.6
pos. 6.6/FANCY-I	3.65	28.1	12.3	30.7	21.3
pos. 6.6/FANCY-II	2.85	25.3	9.69	27.6	20.2
relative decrease(%):	22±21	10±2.5	21±9	10±4	5±5
pos. 6.8/I	4.86	20.8	8.74	21.1	12.3
pos. 6.8/II	3.66	16.5	7.74	18.2	9.9
relative decrease(%):	25±15	21±23	11±10	14±4	20±9
pos. 8.8/I	2.10	14.9	5.17	12.2	7.55
pos. 8.8/II	1.61	11.2	4.51	10.3	5.64
relative decrease(%):	23±21	25±2.6	13±10	16±4.6	25±10

Table VII. Flux level per unit lethargy at some positions in FANCY-I and FANCY-II.
(For clearness sake the standard deviations are given only for the relative flux decrease and not for the separate flux values).

For neutrons with intermediate energy (between 50 keV and 400 keV) the polyethylene rod is physically equivalent to a superposition of a *black absorber* and an *isotropic source*. The first property is due to both the small mean free path of neutrons (about 1 cm) compared to the mean chord length in the rod (4 cm) and the strong moderation by the hydrogen nuclei which implies that almost all neutrons during their passage in the rod are strongly degraded in energy. The second property is a consequence of the fact that approximately all neutrons which leave the rod with an energy in the range considered, have suffered multiple collisions through which the neutrons "forget" the anisotropy in their angular distribution when entering the rod.

For the energy range covered by the measurements, the neutron absorption exceeds the neutron production. The production-to-absorption ratio increases with decreasing energy and exceeds unity at an energy between 100 eV and 1 keV, according to the calculations; on the basis of the previous analysis it is expected that the cross-over point is positioned at higher energy. Concerning the influence of the polyethylene rod on the effective group cross sections for the region surrounding the rod, it is useful to discuss the "source effect" and the "absorber effect" separately.

As a consequence of the scattering of the neutrons inside the rod, the neutrons leaving the rod have a smooth energy spectrum, which implies that the fine structure of the spectrum near the rod is less pronounced than without the moderating material; therefore, near the rod surface more "dilute" cross sections (see Chapter IV) are appropriate.

The "absorber effect" is quite different from the source effect. Local absorption of neutrons leads to a flux depression which extends over a distance comparable to the mean free path of the neutrons concerned; moreover, the relative flux depression at the surface of the absorber becomes smaller with increasing neutron mean free path, which is known from elementary neutron transport theory [Bw64]. This implies that near the absorber the flux in the "valleys" of the spectrum is diminished more than in the maxima; therefore, as a consequence of the insertion of the absorbing material, the self-shielding of the cross section resonances is *increased* near the absorber and *decreased* at some larger distance from the absorbing material. In the terms of the σ_o-concept, described in

Chapter IV, this means that σ_o is negative at the absorber surface, becomes positive at some distance and returns to zero for distances large compared to the mean free path of the neutrons. This model is valid for infinite media; in actual systems the neutronic behaviour is more complicated due to leakage effects.

For the system studied here, the absorption effect exceeds the production effects in the energy range considered, which means that "excess self-shielding" occurs near the polyethylene rod. In assembly position 6.6 this effect is found experimentally, as can be seen from Table VII. For the other positions this effect can not be found, however one should realize that the spectrum in these positions is strongly influenced by the graphite reflector. On the basis of the discussion presented before, it is expected that the effect of "excess self-shielding" can be measured more succesfully in an unreflected aluminium core. Moreover, calculations indicate that by decreasing the graphite reflector thickness, the cross-over point in the perturbation spectrum for polyethylene (for the present system positioned between 100 eV and 1 keV) can be shifted to higher energies, which is interesting from the view-point of experimental verification.

The effect of *excess self-shielding* has been verified with a fine group calculation on the one-dimensional model of FANCY-I; the group structure is the same as described in paragraph V.2.4, the geometry of this model has been described in V.2.1. In Fig. 39 the space-dependence of the ratio between the fluxes in two energy intervals is shown.

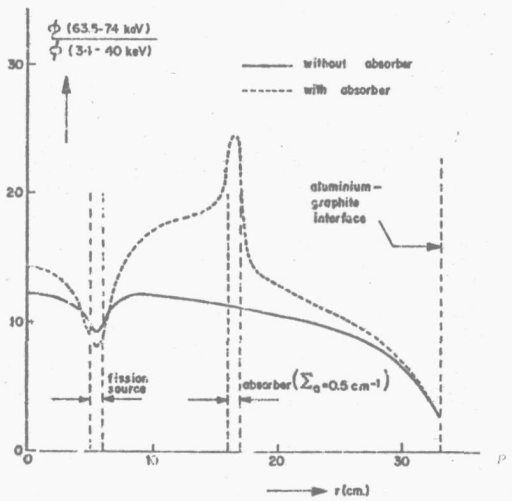

Fig. 39.
Increase of resonance self-shielding caused by the introduction of absorbing material; one-dimensional model of FANCY with a fictitious absorber.

One of these intervals has been selected at the maximum of the 35 keV resonance, the other is selected in the minimum of the cross section curve between the 35 keV resonance and the 88 keV resonance (Fig. 16). The solid line refers to the FANCY-I model, the dashed line is valid for the case, that a shell of a fictitious purely absorbing material with an energy-independent macroscopic absorption cross section equal to 0.5 cm^{-1} has been introduced; the absorbing zone extends from r=16 cm to r=17 cm. The insertion of the absorbing material causes a considerable enhancement of resonance self-shielding, in particular in the "upstream" direction from a neutron point-of-view; in the outer zone of the core the influence of the graphite reflector is evident. It is noticeable that in the fission source zone self-shielding is diminished compared to the system without absorber; this is due to the fact that the relative contribution of first-flight source neutrons to the flux in this region is increased as a consequence of increased neutron capture in the system.

Figures 40, 41 and 42 show the results of perturbation measurements and calculations for the case of insertion of graphite elements. Because in this case the flux changes are only a few percent, it is very difficult to obtain experimental data with sufficient accuracy.

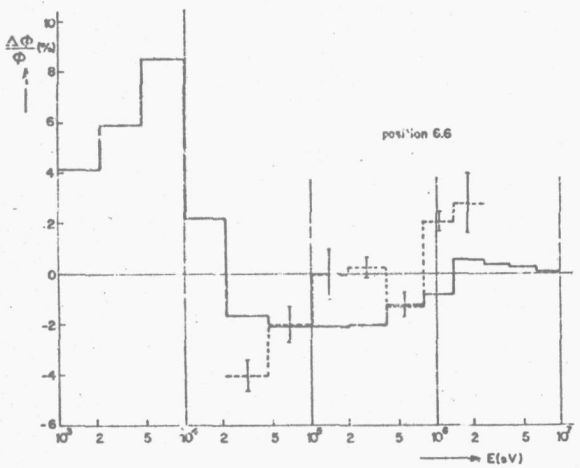

Fig. 40. Calculated (solid line) and measured relative flux perturbation caused by the insertion of graphite elements in FANCY-I, position 6.6.

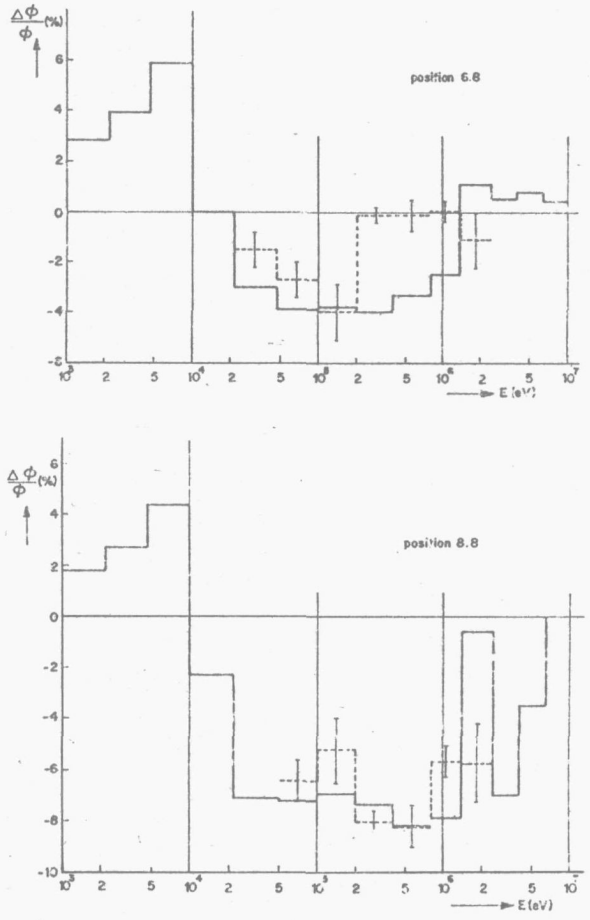

Figs. 41 and 42. Calculated and measured relative flux perturbations caused by the insertion of graphite elements in FANCY-I, positions 6.8 and 8.8.

The calculations indicate a flux enhancement in the MeV region in positions 6.6 and 6.8, which can be attributed to the fact that the scattering cross section in graphite is higher than in aluminium and, additionally, the angular distribution of scattering by graphite nuclei is less forwardly peaked than by aluminium nuclei. Consequently

the high-energy flux in position 8.8 ("downstream" from a neutron point-of-view) is diminished. This effect is more pronounced for the measured 1.4 MeV-2.5 MeV flux, whereas the calculations give in all positions an underprediction of the 0.8 MeV-1.4 MeV flux. In the energy region from 200 keV to 800 keV it is remarkable that no significant flux change is detected in positions 6.6 and 6.8, where as the flux shift in position 8.8 is comparatively large and in good agreement with calculated values. It should be kept in mind however, that the error margins indicated do not account for systematic errors. Because the experimental values for the flux perturbations in *one* position only are the results from measurements extending over a period of 1-2 weeks, it is evident that the systematic errors are probably such that no significance can be attributed to the discrepancies between theory and experiment for the positions 6.6 and 6.8.

For all measurements of flux perturbations, either by detector channels or by moderating materials, *each* measurement was preceded by a measurement of the unperturbed flux, which implies that the measurements in FANCY-I were repeated many times; the reproducibility of the group flux values, derived from these measurements, amounted to 2%.

REFERENCES.

Ab 64 L.P. Abagyan et al.:
Group Constants for Nuclear Reactor Calculations, New York (1964).

An 63 ANL - 5800, Reactor Physics Constants, USAEC 1963.

An 68 ANL - 7394, Analysis and Reduction of Proton Recoil data, by E.F. Bennett, R. Gold and I.K. Olson. p. 72

Be 62 E.F. Bennett. Gamma Ray Discrimination in a Proton-Recoil Proportional Counter. ANL - 6480. March 1962.

Be 64 P.W. Benjamin, C.D. Kemshall and J. Redfearn. The use of a Gas-filled Proportional Counter for Neutron Spectrum Measurements in a Zero Energy Fast Reactor. AWRE Report No. NR 2/64.

Be 67 E.F. Bennett: Fast Neutron Spectroscopy by Proton-Recoil Proportional Counting. Nucl.Sc.Eng.27 (1967) 16.

Be 68 E.F. Bennett, R. Gold and I.K. Olson. Analysis and Reduction of Proton-Recoil Data. ANL - 7394 (1968).

Be 70 E.F. Bennett. Electric Field Effects in Proportional Counters and Their Influence on Spectroscopy, ANL - 7610 (1970).

Br 69*) H. Bruggeman and H. van Dam. Fast - DSN - Delft. Report THD-H-RF-121, Delft (1969).

Bw 64 K.H. Beckurts and K. Wirtz. Neutron Physics. Springer Verlag, Berlin, (1964).

Ca 55 B.G. Carlson. Solution of the transport equation by S_n approximations. LA - 1891. (1955)

Ca 59 B.G. Carlson. Numerical solution of transient and steady-state neutron transport problems. LA - 2260. (1959).

Ca 60 B.G. Carlson et al. The DSN and TDC neutron transport codes. LAMS - 2346. (1960).

Ca 62 R.M. Cantwell. MO176 - A Fortran Program to solve several P-approximations to the few group neutron transport equation in slab geometry. WAPD-TM-320. (1962).

Ca 67 R.W. Campbell et al.: Compilation, Evaluation and Reduction of Neutron Differential Scattering Data, Vol. IV, NAA-SR-11980. (1967).

Ca 68 L.M. Caspers. Comparison between measured and calculated stationary thermal neutron spectra in heterogeneous systems.
Thesis Delft University of Technology. (1968).

Da 66 W.G. Davey. Intercomparison of Calculations for a Dilute Plutonium fueled Fast Critical Assembly (ZPR-3 Assembly 48). Proc. Conf. on Fast Critical Experiments and their Analysis. ANL - 7320 (1966).

Da 67*) H. van Dam. Fast-Zoom-Delft, A Computer Code in Algol for one-dimensional Multigroup Diffusion Calculations. Report THD-H-RF-112, Delft (1967).

Da 68 H. van Dam. Some Remarks on Group Cross Sections for Mixtures with a Resonance-Scattering Component. Nukleonik, 11 (1968) 298.

Dr 60 L. Dresner. "Resonance Absorption in Reactors", Pergamon Press, Oxford (1960).

Du 66 G.J. Duffy et al.: SNARG-1D, A one-dimensional, discrete-ordinate transport theory program for the CDC-3600. ANL - 7221 (1966).

Fa 47 U. Fano. Ionization Yield of Radiations II. The fluctuations of the number of ions. Phys.Rev. 72 (1947) 26.

Fa 66 U. Fano. Electron Multiplication process in proportional counters. Phys.Rev. 147 (1966) 201.

Fa 68 A. Fabry and P. van de Plas. Generation of intermediate standard neutron spectra and their application in fast reactor physics. Fast Reactor Physics, vol. I, p.389, IAEA, Vienna 1968.

Fi 70 E.A. Fisher et al. Physics Investigations of Steam-Cooled Fast Reactor Cores with a Plutonium Fueled Central Zone. SNEAK-Assembly 3B. KFK 1266 (1970).

Ga 64 J.B. Gang et al. Results of measurements (Columbia, 1964) are presented in Ref. [St64].

Gi 53 A.B. Gillespie. Signal, Noise and Resolution in Nuclear Counter Amplifiers. McGraw-Hill Book Co., New York, 1953.

Gr 69 S. Greenbergen, J.M. Outtler, S. Shalev. Optimizing Pulse-Height Risetime Analysis. Trans. Am. Nucl. Soc. 12, nr. 1, 64 (1969).

Hi 59 C.T. Hibdorn. Phys. Rev. 114 (1959) 179.

Ho 70*) P.J. 't Hoen and H. van Dam. XYSNI, An Algol Code for the Solution of the Multigroup Neutron Transport Equation for x-y-geometry on the IBM 360/65 of the Dleft University of Technology. Report IRI-131-70-03, Delft (1970).

Hu 68 P.J. v.d. Hulst. Enige berekeningen en metingen aan verstorende effecten bij de meting van snelle neutronen-spectra met de terugstootprotonen methode. Afstudeerverslag TH Delft, 1968.

Jo 63 G.D. Joanou and A. Halim Kazi. The validity of the transport approximation in fast-reactor calculations. Trans.Am.Nucl.Soc.6, 1 (1963) 17.

Ki 60 R.W. Kiser. Characteristic parameters of gas-tube proportional counters. Appl. Sci.Res.8, section B, 183 (1968).

La 68 J.M. Larson and J.E. Powell. Electronic System Developments for Proton Recoil Spectra Measurements in Plutonium Critical Facilities. Trans. Am. Nucl. Soc., 11 (1968) 635.

La 68 K.D. Lathrop. "Ray Effects in Discrete Ordinate Equations". Nucl. Sc. Eng. 32 (1968) 357.

Le 62 C.E. Lee. The discrete S_n approximation to transport theory. LA - 2595 (1962).

Le 70 G. de Leeuw and S. de Leeuw (C.E.N. Mol,Belgium). Private communication.

Ma 60 J.B. Marion and J.M. Fowler (eds.). Fast Neutron Physics, Part I, New York 1960.

Me 66 D. Meneghetti. Effects of Leakage Upon Evaluation of Fast Reactor Multigroup Cross Sections for Reflectors. ANL - 7170 (1966).

Mi 70 L.B. Miller and R.E. Jarka. The Importance of Discrete-Ordinate Ray Effects in Fast Reactor Design Studies. Trans.Am.Nucl.Soc. 13, 2 (1970) 629.

No 65 C.H. Nowling and J.L. Blankenship. Elimination of Undesirable Undershoot in the Operation and Testing of Nuclear Pulse Amplifiers. Rev. Sci. Instr. 36, 1830 (1965).

Ok 55 D. Okrent et al. A Survey of the Theoretical and Experimental Aspects of Fast Reactor Physics. Proc. UN Intnl. Conf. on Peaceful Uses of Atomic Energy, Geneva, 5, 347 (1955).

Pa 63 J.B. Parker, P.H. White and R.J. Webster. The interpretation of recoil proton spectra. Nucl. Instr. Meth. 23 (1963) 61.

Pa 68 W.J. Paterson, P.W. Benjamin, D. Hatton, W.B. McCormick and J.W. Weale. Neutron Spectrum measurements in the fast reactor assembly VERA 19A and tests of the time-of-flight spectrometry method in VERA 5A and VIPER 1. Fast Reactor

Physics, Vol. II, p.113, IAEA, Vienna 1968.

Pe 62 E.D. Pendlebury and L.H. Underhill. The validity of the transport approximation in critical-size and reactivity calculations. Physics of Fast and Intermediate Reactors, Vol. II, p.73, IAEA, Vienna (1962).

Pr 64 W.J. Price. Nuclear Radiation Detection. McGraw-Hill Book Company, New York, 1964.

Ra 63 G. Rakavy and Y. Yeivin. The transport approximation of the energy dependent boltzmann equation. Nucl. Sc. Eng. 15 (1963) 158.

Ra 64 A.L. Rago and H.H. Hummel. ELMOE, An IBM-704 Program Treating Elastic Scattering Resonances in Fast Reactors. ANL - 6805 (1964).

Ra 65 V. Radeka. Low Noise Preamplifiers for Nuclear Detectors. Nucleonics 23, no. 7, 52 (1965).

Ro 49 B.B. Rossi and H.H. Staub. Ionization Chambers and Counters, page 91. McGraw-Hill Book Co., New York, 1949.

Ro 64 M.L. Roush, M.A. Wilson and W.F. Hornyak. Pulse Shape Discrimination. Nucl. Instr.Meth. 31 (1964) 112.

Sn 61 I.N. Sneddon. Special Functions of Mathematical Physics and Chemistry. Interscience Publishers, New York, 1961.

Sn 67 N.L. Snidow and H.D. Warren. Wall effect corrections in proportional counter spectrometers. Nucl. Instr. Meth. 51 (1967) 109.

So 67 B. Soucek and R.L. Chase. Tunnel diode pulse shape discrimination Nucl. Instr. Meth. 50 (1967) 71.

St 64 J.R. Stehn et al. Neutron Cross Sections, Vol. I, Sec. Ed., Suppl. 2, BNL-325 (1964).

St 65 M.G. Strauss and R. Brenner. General Purpose Analog Pulse Height Computer. Rev. Sci. Instr. 36 (1965) 1857.

To 67 B.J. Toppel, A.L. Rago and D.M. O'Shea. MC^2 - A code to Calculate Multigroup Cross Sections. ANL - 7318 (1967).

Wa 68 LMFBR - Liquid Metal Fast Breeder Reactor Program Plan. WASH 1101-1110.

We 58 A.M. Weinberg and E.P. Wigner. The Physics Theory of Neutron Chain Reactors. The University of Chicago Press, Chicago (1958).

Wi 68 C.W. Williams. Reducing Pulse Height Spectral Distortion by Means of DC Restoration and Pile-up Rejection. IEEE Trans. Nucl. Sci., NS-15. No. 1, 297 (1968).

*) The THD- and IRI-reports mentioned in this reference list can be obtained from the Reactor Physics Group, Interuniversity Reactor Institute, Delft, The Netherlands.

LIST OF SYMBOLS AND ABBREVIATIONS.

A	mass number	
B^2	flux buckling	m^{-2}
E	energy of neutron c.q. proton	eV
E_n	neutron energy	eV
f	self-shielding factor	
F	neutron collision density	$cm^{-3}.s^{-1}$
g	group number	
K(E,E')	probability for a recoil-proton with initial energy E to be detected per unit energy interval at E'	eV^{-1}
ℓ	track length of recoil-proton	cm
ℓ(index)	order of Legendre polynomial c.q. component	
L	length of sensitive volume of a detector	cm
LHS	left-hand side	
m	order of Legendre polynomial c.q. component	
M(E)	neutron flux spectrum calculated without accounting for carbon recoils	$cm^{-2}.s^{-1}.eV^{-1}$
n_i	number of counts in channel i of the multichannel analyzer	
N	number of protons in the sensitive volume of a detector	

$N(x,\mu)$	neutron flux density per unit μ-interval about the direction μ at x	$cm.^{-2}s^{-1}$
$P(E)$	proton spectrum corrected for wall effects	$eV^{-1}.s^{-1}$
$P'(E)$	measured proton spectrum	$eV^{-1}.s^{-1}$
Q	neutron source density	$cm^{-3}.s^{-1}$
R	radius of sensitive volume of detector	cm
RHS	right-hand side	
$S(x,\mu)$	source of neutrons per unit volume per unit μ-interval about the direction μ at x	$cm^{-3}.s^{-1}$
u	neutron lethargy	
w_i	relative intrinsic width, indicating detector resolution	
x	space coordinate	m
α	neutron energy after collision relative to energy before collision	
α^c	α-value for carbon	
α^{al}	α-value for aluminium	
Γ_t	total resonance width	eV
Γ_n	resonance width for scattering	eV
Δu	group width in lethargy units	
η	azimuthal angle between neutron flight directions before and after scattering	

μ	cosine of the angle between the coordinate axis and the neutron flight direction c.q. cosine of scattering angle	
μ_o	mean cosine of scattering angle	
ξ	mean logarithmic energy decrement (= lethargy gain) per collision	
σ	microscopic cross section	cm^2
σ_c	carbon scattering cross section	cm^2
σ_H	hydrogen scattering cross section	cm^2
σ_o	background total cross section per resonant atom, used for self-shielding calculations	cm^2
σ_{rel}	relative standard deviation	
Σ	macroscopic cross section	cm^{-1}
Σ_d	macroscopic slowing-down cross section	cm^{-1}
$\Sigma_\ell^{g'g}$	ℓ-th Legendre component of the macroscopic cross section for scattering from group g' to group g	cm^{-1}
Σ_{rem}	macroscopic removal cross section	cm^{-1}
Σ_s	macroscopic scattering cross section	cm^{-1}
Σ_{str}	macroscopic transport cross section for scattering	cm^{-1}

Σ_t	macroscopic total cross section	cm^{-1}
Σ_{tr}	macroscopic transport cross section	cm^{-1}
ϕ	neutron flux density	$cm^{-2}.s^{-1}$
$\phi(E)$	neutron flux per unit energy	$cm^{-2}.s^{-1}.eV^{-1}$
$\phi(u)$	neutron flux per unit lethargy	$cm^{-2}.s^{-1}$
ϕ_{ℓ}^{g}	ℓ-the Legendre component of neutron flux in group g	$cm^{-2}.s^{-1}$

SUMMARY

In this thesis a theoretical and experimental analysis of fast neutron spectra is presented, with emphasis on resonance scattering effects and the influence of anisotropic scattering on the space-energy distribution of neutrons.

In the first Chapter the relationship between neutron energy distributions and fast reactor system parameters, with regard to economics and safety, is discussed after a historical sketch of nuclear reactor development.

In the second Chapter a description is given of the FANCY-assembly which is positioned adjacent to the HOR pool-type reactor at Delft and has been used for experimental verification of computer calculations on space-dependent spectra in aluminium. This Chapter comprises an analysis of incore fast neutron spectrometry by means of proton-recoil proportional counters. After an outline of the principles of this method, attention is given to some characteristics of the detectors, advantages and disadvantages of spherical respectively cylindrical detectors and to different methods of energy calibration. An analysis is presented of the data reduction optimization from proton-recoil spectra in view of counting statistics and energy resolution. Further a method has been developed for correction of wall effects, which occur as a consequence of the finite dimensions of the detectors. Electronic circuitry for gamma discrimination, based on new principles, was developed and some experimental results are presented. These results demonstrate the good discrimination capabilities of the system.

In the third Chapter the neutron transport equation is analyzed in some detail with special emphasis on the treatment of anisotropic scattering. First the one-group theory is treated; for this case the definition of transport corrected cross sections, which are used to deal with anisotropic scattering, is shown to be unambiguous. For the multigroup (i.e. energy-dependent) case different approaches are possible. An analysis is presented of the physical background of three concepts, i.e. the diagonal

transport approximation, the corrected diagonal transport approximation and the modified diagonal transport approximation. The ranges of applicability of these concepts are studied and on the basis of calculations for a particular system the attainable accuracies are illustrated for the different approximations.

Both diffusion and S_n computer codes were developed and the discrepancies to be expected between the results of diffusion codes and more advanced concepts, such as S_n-codes, are explained. For the study of the influence of anisotropic scattering on neutron energy distributions a special S_n- code was developed, which can handle the anisotropy of scattering distributions with a high degree of accuracy.

In Chapter IV a discussion is given of group cross section evaluation. For both diffusion and transport calculations group cross section definitions are derived. It is shown that, in order to eliminate the angular dependence of group cross sections, it is necessary to base the group cross section definitions for transport calculations on a less rigorous approximation of the transport equation which then leads to the same group cross section definitions for diffusion and transport calculations. It is emphasized that standard group cross section sets are *a fortiori* based on particular averaging spectra which consequently requires careful application of these sets. Results of group cross section calculations for mixtures of a resonance scatterer and a potential scatterer are presented. It is shown that the use of tables of self-shielding factors leads to erroneous results, in particular for slowing-down cross sections. A discussion is given of the influence of neutron leakage on group cross section values and a method is presented which can be used either for improvement of the accuracy of calculations of space-dependent neutron spectra or for the procurement of group cross sections from measured spectra.

The final Chapter contains the results of calculations and measurements of neutron energy distributions in the FANCY-assembly. Results of one-dimensional diffusion and S_n calculations are presented; the differences in spectra obtained with these methods are explained on the basis of an analysis given in Chapter III. The influence of anisotropic scattering on the neutron spectra in FANCY is studied. It is shown that

transport approximations give satisfactory results except at positions near the source for neutrons with intermediate energies (0.1 MeV - 1 MeV). A considerable improvement is obtained by inclusion of the first moment of the angular distribution of neutron scattering (P_1-component).

The two-dimensional S_n calculations performed for FANCY led to an analysis of the so-called "ray-effect" which can occur near strong heterogeneities (such as neutron sources or absorbers) as a consequence of the angular discretization used in the S_n method. Two methods for elimination of this effect are indicated: an increase of the order of the angular quadrature, which led to the incorporation of group-dependent order of angular quadrature in the code developed for the two-dimensional analysis, and *group-collapsing* of the high energy groups. The latter method has the advantage of a considerable decrease of computer time but has a limited applicability.

Space dependence of group cross sections in FANCY has been studied and the results of the calculations are explained on the basis of the space dependence of resonance self-shielding which is caused by the presence of the fission source and the graphite reflector. The use of space-*in*dependent cross sections can lead to considerable errors in spectrum prediction but in some cases the different influences of changes in the transport respectively the slowing-down cross section lead to a partial cancellation of errors.

After a discussion of some experimental aspects the results of measurements in the FANCY-core are presented and compared to one- resp. two-dimensional calculations. For the intermediate part of the spectrum the one-dimensional approximation looks adequate, whereas for the energy groups above 800 keV the flux gradient is overestimated by the one-dimensional approximation and underestimated by the two-dimensional model, which is caused by the discrepancy between the actual source geometry and the idealized source geometries used in the calculations. A discussion is given of the group cross section values inferred from the FANCY-measurements. The agreement of these experimental values with the theoretical results of fine group calculations is satisfactory, except for the energy group between 100 keV and 200 keV, where the slowing-down cross section is strongly affected by a

rather narrow resonance peak near the lower group boundary; the width of this resonance peak is such that more detailed fine group calculations seem to be necessary to give a correct prediction of the space-dependent spectral behaviour.

Flux perturbations caused by detector channels are calculated and explained qualitatively; the experimental results indicate that the geometry of the system has been oversimplified in the two-dimensional calculations. The same conclusion can be inferred from the comparison between calculations and measurements of flux perturbations caused by the local insertion of moderating materials, i.e. polyethylene and graphite. For the flux perturbation by graphite the agreement between calculations and experiment is satisfactory within the limits of the experimental accuracy, for the flux perturbation by polyethylene the *energy-dependence* is predicted rather well by the calculations but the absolute value of the flux shift is overpredicted by a factor of 2 to 3, depending on the position in the core.

For the flux perturbation caused by polyethylene as qualitative analysis is presented which leads to the introduction of an effect, which we indicated as "excess self-shielding". This name has been given to the phenomenon, that the local introduction of strongly absorbing or moderating material in a system of nuclides exhibiting resonance scattering gives rise to an enhancement of the energetic resonance self-shielding. This effect is demonstrated on the basis of calculations on the one-dimensional model of FANCY and has been found as a result of the analysis of the changes in the detailed neutron spectra in FANCY, caused by the insertion of polyethylene rods.

SAMENVATTING

In dit proefschrift wordt een theoretische en experimentele analyse gegeven van snelle neutronen spectra, waarbij in het bizonder aandacht wordt besteed aan de invloed van resonantieverstrooiing en anisotrope verstrooiing op de plaatsafhankelijke energieverdeling van neutronen.

In het eerste hoofdstuk wordt, na een historische schets van de kernreactorontwikkeling, de aandacht gevestigd op het verband tussen de energieverdeling van neutronen in snelle reactoren en de voor de economie en de veiligheid van belang zijnde systeemparameters.

In het tweede hoofdstuk wordt een beschrijving gegeven van het FANCY-ensemble, dat geplaatst is bij de Hoger Onderwijs Reactor te Delft en gebruikt is voor meting van plaatsafhankelijke neutronenspectra in aluminium. Verder bevat dit hoofdstuk een analyse van neutronenspectrometrie met behulp van terugstootprotonen-telbuizen. Na een beschrijving van de principes van deze metode voor neutronenspectrometrie wordt aandacht besteed aan telbuiskarakteristieken, voor- en nadelen van bolvormige respectievelijk cilindervormige detectoren en aan verschillende ijkmethoden. Een analyse wordt gegeven op welke wijze optimale informatie wordt verkregen uit gemeten energieverdelingen van terugstootprotonen in verband met telstatistiek en de energieresolutie van de gebruikte detectoren. Voorts wordt een metode uiteengezet voor het korrigeren van meetresultaten voor randeffekten, die optreden ten gevolge van de eindige detectorafmetingen. Een nieuwe metode voor gammadiscriminatie langs electronische weg wordt beschreven en enige experimentele resultaten worden getoond, die het goede discriminerende vermogen van de gebruikte apparatuur demonstreren.

In het derde hoofdstuk wordt de transportvergelijking voor neutronen geanalyseerd, waarbij enige nadruk valt op de behandeling van anisotrope verstrooiing. Eerst wordt de z.g. ééngroepstheorie behandeld; aangetoond wordt dat voor dit geval de definitie van de transportwerkzame doorsnede, die gebruikt wordt voor het benaderend in rekening brengen van anisotrope verstrooiing, éénduidig is. Bij de meergroepstheorie zijn verschillende benaderingen mogelijk. Een analyse wordt gegeven van de

fysische achtergrond van drie mogelijke benaderingen: de diagonale transport benadering, de gekorrigeerde diagonale transport benadering en de gemodificeerde diagonale transport benadering. Het toepassingsgebied van deze benaderingen wordt aangeduid en aan de hand van berekeningen aan een modelensemble wordt de nauwkeurigheid van de verschillende benaderingen geillustreerd.

Voor de theoretische ondersteuning van het in dit proefschrift beschreven werk werden diffusie- en S_n - rekenprogramma's ontwikkeld. In het derde hoofdstuk wordt geanalyseerd welke verschillen te verwachten zijn tussen de uitkomsten van diffusiecodes en meer geavanceerde transportcodes. Ter bestudering van de invloed van anisotrope verstrooiing op de energieverdeling van snelle neutronen werd een speciale S_n-code ontwikkeld waarmee anisotrope neutronenverstrooiing met een hoge graad van nauwkeurigheid in rekening kan worden gebracht.

In hoofdstuk IV wordt een beschouwing gegeven van de berekening van groepsdoorsneden. Groepsdoorsnededefinities voor diffusie- en transportberekeningen worden afgeleid. Er wordt aangetoond dat, ter vermijding van hoekafhankelijkheid van groepsdoorsneden, het noodzakelijk is de definitie van groepsdoorsneden voor transportberekeningen te baseren op diffusietheorie. Benadrukt wordt dat z.g. standaard-doorsnedesets gebaseerd zijn op bepaalde weegspectra, waardoor voorzichtigheid in de toepassing van deze sets geboden is. Groepsdoorsneden voor een mengsel van een resonantieverstrooier en een potentiaalverstrooier zijn berekend en worden in het vierde hoofdstuk bediscussieerd. Aangetoond wordt dat het gebruik van standaardtabellen van zelfafschermingsfactoren tot foutieve resultaten leidt, in het bizonder voor moderatiedoorsneden. Voorts wordt de invloed van neutronenlek op groepsdoorsneden nagegaan en een metode wordt aangegeven om de nauwkeurigheid van berekeningen van plaatsafhankelijke neutronenspectra te vergroten òf werkzame doorsneden af te leiden uit gemeten spectra.

Het laatste hoofdstuk bevat de resultaten van berekeningen en metingen van neutronenspectra in het FANCY-ensemble. Resultaten van ééndimensionale diffusie- en S_n-berekeningen worden bediscussieerd en de invloed van anisotrope verstrooiing op de energieverdeling van neutronen in FANCY wordt nagegaan. Het blijkt dat toepassing van transportbenaderingen tot bevredigende

resultaten leidt met uitzondering van het spectrale gedrag in het energiegebied van 100 keV tot 1 MeV op korte afstanden van de neutronenbron. De z.g. P_1-benadering, waarbij de hoekafhankelijke verstrooiing wordt beschouw als lineair anisotroop, is aanzienlijk nauwkeuriger.

De tweedimensionale S_n-berekeningen die voor het in dit proefschrift beschreven onderzoek werden uitgevoerd hebben geleid tot een nadere bestudering van het z.g. "ray-effect" dat bij sterke heterogeniteiten (zoals neutronenbronnen en neutronenabsorbers) kan optreden als gevolg van de hoekdiscretisatie die bij S_n-berekeningen wordt toegepast. Twee metoden voor het verkleinen van dit effect worden aangegeven: een vergroting van het aantal discrete richtingen voor de vectoriële neutronenfluxdichtheid of groepscondensatie, d.w.z. het samenvoegen van groepen. Teneinde de eerste metode optimaal te kunnen toepassen, kan in de ontwikkelde rekencode voor iedere groep de gewenste hoekdiscretisatie worden gespecificeerd. De tweede metode heeft als voordeel een aanzienlijke rekentijdbekorting maar is beperkt toepasbaar.

De plaatsafhankelijkheid van groepsdoorsneden in FANCY is bestudeerd en wordt kwalitatief verklaard aan de hand van de plaatsafhankelijke zelfafscherming van resonanties die een gevolg is van de aanwezigheid van de grafietreflector en de neutronenbron. Het gebruik van plaatsonafhankelijke groepsdoorsneden kan leiden tot aanzienlijke afwijkingen in de berekende spectra, maar in sommige gevallen geven de verschillende invloeden van de fouten in de transport- respectievelijk de moderatiedoorsneden aanleiding tot een gedeeltelijke opheffing van fouten.

Na een discussie van enige experimentele aspecten worden de meetresultaten voor de FANCY-kern vergeleken met de resultaten van één- en tweedimensionale berekeningen. Voor het intermediaire deel van het spectrum blijkt de ééndimensionale benadering bevredigend te zijn, terwijl voor de groepen boven 800 keV de fluxgradiënt overschat wordt door de ééndimensionale benadering en onderschat door de tweedimensionale benadering, hetgeen een gevolg is van de discrepantie tussen de werkelijke brongeometrie en de geïdealiseerde brongeometrieën waarvan bij de berekening wordt uitgegaan. De groepsdoorsneden, die kunnen worden afgeleid uit de

FANCY-metingen geven een redelijke overeenkomst te zien met de resultaten van meergroepsberekeningen met verfijnde energiediscretisatie in het intermediaire energiegebied. Een uitzondering blijkt de groep tussen 100 keV en 200 keV te zijn, waar de moderatiedoorsnede in belangrijke mate wordt beinvloed door een vrij smalle resonantiepiek nabij de ondergrens van de groep. De breedte van deze rezonantiepiek is zodanig dat berekeningen met nog verder verfijnde energiedetaillering noodzakelijk schijnen te zijn teneinde het plaatsafhankelijke spectrum korrekt te voorspellen.

Fluxverstoringen, veroorzaakt door meetkanalen, zijn berekend en worden kwalitatief verklaard; de meetresultaten tonen aan dat de geometrie van het systeem te sterk vereenvoudigd is bij de tweedimensionale benadering. Dezelfde conclusie kan worden getrokken uit de vergelijking van berekende en gemeten fluxveranderingen ten gevolge van de plaatselijke introductie van modererende materialen, in dit geval grafiet en polyethyleen. Voor de energieafhankelijke fluxveranderingen, veroorzaakt door grafietstaven, is de overeenstemming tussen berekening en meting bevredigend, gezien de beperkte meetnauwkeurigheid bij de hier optredende kleine veranderingen. Van de fluxveranderingen, veroorzaakt door polyethyleenstaven, wordt de *energieafhankelijkheid* goed berekend maar de absolute grootte wordt met een factor 2 à 3, afhankelijk van de positie waarin gemeten is, overschat.

Voor de fluxverstoring veroorzaakt door polyethyleen wordt een kwalitatieve analyse gegeven, die leidt tot de introductie van een effect dat in dit proefschrift wordt aangeduid als "excess self-shielding". Deze naam is hier gegeven aan het verschijnsel dat de plaatselijke introductie van een sterk absorberend of modererend materiaal in een systeem met één of meerdere resonantieverstrooiers een vergroting van de resonantiezelfafscherming veroorzaakt. Dit effect wordt gedemonstreerd aan de hand van berekeningen aan het ééndimensionale model van FANCY en is gevonden als resultaat van een analyse van de veranderingen in de fijnstructuur van de FANCY-spectra, die veroorzaakt worden door het inbrengen van polyethyleenstaven.

ACKNOWLEDGEMENTS

H. Bruggeman, P.J. 't Hoen, P.J. v.d. Hulst and A.F.B. Reyngoud participated as students in various parts of this study while fulfilling the requirements for the degree of Natuurkundig Ingenieur. Their contribution is gratefully acknowledged.

Further I am indebted to dr. H.R. Kleijn and other members of the Reactor Physics Group for valuable discussions. Thanks are due to the technical staff, in particular to R.P.R. Gaal, for skillful experimental assistance.

Finally, I would like to thank the members of the Reactor Division of the Interuniversity Reactor Institute at Delft for their pleasant cooperation and Mrs. M. Rutgers and Miss H.J.Prins for typing the manuscript.

STELLINGEN

1. Intermediaire reactoren met hybriede splijtstofcyclus (^{233}U-^{238}U-^{232}Th) vereisen een aanzienlijk lagere specifieke splijtstofinvestering dan snelle reactoren met een plutoniumcyclus, terwijl bovendien de voor de veiligheid van belang zijnde reactiviteitskoëfficienten gunstiger zijn.

   Litt.: H. van Dam and J.J. Went: Thorium Cycle Breeder Reactors, Atompraxis 3 (1969) 173.

2. Een kombinatie van snelle kweekreactoren met thoriummantel en thermische "bijna-kweek"-reactoren met ^{233}U-splijtstof biedt een grote flexibiliteit in het realiseren van een gewenst groeipercentage van de nucleaire energievoorziening.

3. De noodzakelijkheid van het uitgebreid toepassen van statistische test-methoden op de reeks van Fibonacci maakt deze reeks tot een zeer twijfelachtige generator van rechthoekig verdeelde aselecte getallen.

   Litt.: Symposium on Monte Carlo Methods, held at University of Florida, 1954, edited by H.A. Meyer (Wiley, New York, 1956).

4. Het is onjuist te stellen dat de duur van neutronendiffractiemetingen omgekeerd evenredig is met het vermogen van de daarvoor gebruikte reactor.

   Prof.dr. J.A. Goedkoop: Atoomenergie en haar toepassingen, 12 (1970) 243.

5. Het gebruik van beryllium in de tritiumkweekmantel van een D-T-fusiereactor moet worden vermeden. Een betere neutroneneconomie kan worden verkregen door toepassing van uitsluitend lithium of lithiumzouten in kombinatie met een konstruktiemateriaal met hoge (n,2n) werkzame doorsnede.

6. De opmerking van Abagyan e.a., dat bij berekening van de effectieve moderatiedoorsnede voor nucliden met resonanties in de werkzame doorsnede gebruik kan worden gemaakt van de zelfafschermingsfactor voor elastische verstrooiing, is onjuist.

   L.P. Abagyan e.a.: Group Constants for Nuclear Reactor Calculations, New York 1964, pag. 39.

   Hoofdstuk IV van dit proefschrift.

7. De definitie van de "achtergrond"-werkzame doorsnede zoals gegeven door Abagyan e.a., is niet éénduidig voor het geval dat meerdere nucliden met resonanties in de werkzame doorsnede in een systeem aanwezig zijn. Dit heeft aanleiding gegeven tot verschillende interpretaties in de literatuur.

   L.P. Abagyan e.a.: Group Constants for Nuclear Reactor Calculations, New York 1964.
   Rapport BNWL-146 : Red Cross, a code to compute resonance shielded, temperature dependent cross sections for fast reactor analysis. (1965).
   Rapport KFK-1266 : Physics Investigations of steam-cooled fast reactor cores with a plutonium fueled central zone. (1970).

8. Het verdient de voorkeur intermediaire warmtewisselaars voor natriumgekoelde reactoren zodanig te konstrueren, dat de primaire koelvloeistof *door* de pijpenbundel stroomt.

9. De oprichting van een landelijk depot voor hulpmiddelen, die benodigd zijn voor decontaminatie na nucleaire bedrijfsongevallen, is zeer wenselijk.

10. Volgens de huidige stand van de wetenschap is er meer bekend over het nuttig effect van de toevoeging van fluorzout aan drinkwater dan over de schadelijkheid van het eten van aardappels.

    Litt.: Advies inzake de Medisch-Toxicologische en Tandheelkundige aspecten van het fluorideren van drinkwater
    (Advies nr. 19 van de Gezondheidsraad, Staatsuitgeverij, 's-Gravenhage 1970).

H. van Dam

Delft, 23 juni 1971.